

RSC Advances



This is an *Accepted Manuscript*, which has been through the Royal Society of Chemistry peer review process and has been accepted for publication.

Accepted Manuscripts are published online shortly after acceptance, before technical editing, formatting and proof reading. Using this free service, authors can make their results available to the community, in citable form, before we publish the edited article. This *Accepted Manuscript* will be replaced by the edited, formatted and paginated article as soon as this is available.

You can find more information about *Accepted Manuscripts* in the [Information for Authors](#).

Please note that technical editing may introduce minor changes to the text and/or graphics, which may alter content. The journal's standard [Terms & Conditions](#) and the [Ethical guidelines](#) still apply. In no event shall the Royal Society of Chemistry be held responsible for any errors or omissions in this *Accepted Manuscript* or any consequences arising from the use of any information it contains.

Effects of C_{1,3}-doping on Electronic and Structural Properties of Stone-Wales Defective Boron Nitride Nanotubes as well as their NO Gas Sensitivity

Hossein Roohi*, Layla maleki

Department of Chemistry, Faculty of Science, University of Guilan, Rasht, Iran.

Abstract

Doping of nanotubes can be a useful way not only to tune their electronic, optical and magnetic properties, but also to enhance its chemical reactivity and designing nanoelectronic devices. In this work, a first principle exploration was performed to investigate the electronic and structural properties of C-doped Stone-Wales (SW) defective (6,0) single-walled boron nitride nanotubes (BNNTs) at B3LYP/6-31+G(d) and M06-2X/6-31+G(d) levels of theory as well as their chemical sensitivity toward NO gas at ONIOM(M06-2X/6-31++G(d,p):M06-2X/STO-6G) level. The different situations and concentrations of C dopant atoms were explored. The interaction energies and global reactivity descriptors were used to predict the overall reactivity of the studied C-doped SW-BNNTs. The results show that the doping of C at the neighboring B and N sites located in the 7-7 ring fusion (C_{NB} and C_{NBB}) leads to lower defect formation energies. In addition, we find that C impurity is more possible to substitute the boron site due to the low formation energy. Owing to formation of the mid-gap states induced by substituting 3C atoms for three B atoms, a transformation from electrical insulator (band gap of 4.27 eV) to an electrical conductor (band gap of 1.65 eV) is predicted. Therefore, from these results it can be predicted that the 3C_B-doped SW-BNNTs can be used to improve solar cell efficiency. The Results obtained at M06-2X/6-31++G(d,p) level reveal that the NO adsorptions on the surface of C-doped SW-BNNTs are energetically favorable

*Corresponding author. Fax: +98 1333 323262.
E-mail addresses: hrouhi@gmail.com, hroohi@guilan.ac.ir (H. Roohi).

and are stronger than pristine and undoped SW-BNNTs. It is expected that the present results provide a useful guidance to develop novel C-doped BNNTs based sensors for the detection of toxic **NO** molecule.

Key words: BNNT; Stone-Wales defect (SW); C-doping; Electronic properties; DFT; Adsorption; NO gas.

Introduction

BN nanotubes (BNNTs) have the same atomic structure as their carbon nanotubes (CNTs). CNTs with small band gaps (E_g) in the range 0.2–2.0 eV might be either metallic or semiconductor. BNNTs have profound chemical and thermal stabilities and with much wider band gaps of about 5.5 eV are electrically insulating.^{1–5} Due to the thermal issues related to CNTs based devices, it was speculated that BNNTs could be better candidates for nanoelectronic engineering. The large band gap makes the BNNTs as promising materials for a number of potential applications in polymeric composites,⁶ sensors,⁷ catalysts,⁸ molecule based logic gates, nanoelectronics and optoelectronic⁹ devices. Thus, it is especially important to find a way to tune BNNT electronic properties in order to widen the application field. Although some methods have been predicted to be useful for BNNT band gap engineering using theoretical calculations,⁵ in practice, such methods are very difficult to realize due to the extreme conditions involved, such as very high electric field or pressure.

The electronic properties of BN nanotubes e.g. their band gaps can be controlled through a regular mechanism, their ranges of application would be greatly extended, particularly in sensors and nanoelectronics. Various methods including physical methods (such as applying electric field¹⁰ and strain^{11,12}) and chemical methods^{13–15} have been used to tune the electronic properties of BNNTs. The physical methods change directly the band gap while the chemical methods tune the band gap by introducing localized energy level inside the gap¹⁶.

The tuning the electronic properties of NTs can be achieved by doping the nanotube as predicted in theoretical calculations¹⁷⁻²² and found in experimental studies.²³⁻²⁹

A very important topological defect in BNNTs is Stone–Wales (SW) one, which is comprised of two pairs of five-membered and seven-membered rings (5-7-7-5) formed by rotating one bond of the traditional six-membered ring by 90°. ³⁰ Atomistic simulations^{12,31} and experiments^{32,33} have shown that the topological defects (5-7-7-5) in BNNTs generate two unfavorable homoelemental B-B and N-N bonds that increase the total energy of the system. However, formation of these bonds can be prohibited if there is a C–C defect in BNNT. Kim *et al.*³⁴ have studied physical properties of SW-BNNT with the substitutional C pair defect. Jalili *et al.* investigated effect of Stone–Wales defects on structural and electronic properties of zigzag C₃N nanotubes.³⁵ The effect of carbon doping on Stone–Wales defective sites in the armchair BNNTs have been studied by Anafcheh *et al.*³⁶

Nitric oxide (NO) is a toxic free radical gas that is a known bioproduct in almost all types of organisms, ranging from bacteria to plants, fungi, and animal cells.³⁷ Selective reduction of NO in oxidizing atmospheres has recently received much attention because it has potential as a practical measure to remove NO_x emitted from diesel and lean burn engines.³⁸ A very different area, where NO sensing is also required, is in the medical industry, specifically in breath analysis for diagnosis of respiratory ailments.³⁹ Although it has been infamous for its harmful impact on the environment, it's removing and sensing is still a challenging problem. Therefore, reliable and low-cost NO sensors with high selectivity and sensitivity have been required for humans health and environmental safety. Recently great advances have been made in demonstrating the capability of using nanotubes to detect of NO gas. Defected SWCNTs, if embedded in physiological systems, can serve as a sensor for biological NO.⁴⁰ Yates et al.⁴¹ have studied the physical adsorption of NO on purified single-walled carbon nanotubes at low temperatures by means of transmission infrared

spectroscopy. The adsorption of NO molecule on CNTs⁴² and BNNTs⁴³ were theoretically investigated. Rafati et al.⁴² found that a NO molecule can be physisorbed on the surface of CNTs endothermically. Adsorption of CO and NO on the boron site (C_B) and at a nitrogen site (C_N) in the 1C-doped BNNT using local density approach (LDA) has been studied by Baierle *et al.*⁴⁴ They have shown that a chemical bond between the tube and the adsorbed molecule is observed when a carbon substitution impurity is inserted in the tube wall. The chemisorptions of NO and NNO molecules on SiCNTs, CNTs and BNNTs were investigated by Kang et al.⁴⁵ They found that NO and NNO molecules can be chemisorbed on SiCNTs with an appreciable binding energy and that this is not the case for either CNTs or BNNTs. Recently, Chen *et al.*⁴⁶ investigated the adsorption and reduction of NO molecule on the silicon Si-doped graphene. They found that NO can be easily converted into N_2O through a dimer mechanism on Si-doped graphene.

According to our knowledge, there are no theoretical studies on the adsorption of NO molecule on C-doped Stone–Wales defected BNNTs. Recently, we investigated adsorption sensitivity of the perfect and Stone–Wales defective BNNTs towards NO gas by means of DFT method.⁴⁷ Our results showed that the NO adsorptions on the outer and inner surface sites of pristine and SW-BNNTs were energetically favorable and unfavorable, respectively. Besides, NO adsorption on the PS-BNNTs was stronger than that of SW ones. We previously studied the effect of CH_3CO functional group on the molecular and electronic properties of BNNT.⁴⁸ Besides, recently, we have investigated the response of (6,0) BNNT and (6,0) SW-BNNT to axial tension and compression^{49,11} and green chemical functionalization of CNTs with ionic liquids⁵⁰ as well as chemical functionalization of boron nitride nanotube via the 1,3-dipolar cycloaddition reaction of azomethine ylide.⁵¹ In this paper, the effects of C_{1-3} -doping located in different atomic situations of SW defect region on electronic and structural properties of the SW-BNNT are investigated. Moreover, the second part of present work is

devoted to a first-principle investigation of using C-doped SW-BNNT as a sensor and adsorbent of NO molecule. The C-doped SW-BNNTs C_B , C_N , C_{2B} , C_{2N} , C_{NB} , C_{3N} , C_{3B} , C_{2N1B} and C_{1N2B} are considered. The C_B and C_N symbols denote doping of C atom at the B and N sites, respectively. The C atoms substituting for two N atoms and one B atom is abbreviated by C_{2N1B} . The structural parameters, defect formation energy, HOMO–LUMO gap, dipole moment, global reactivity descriptors including chemical potential, chemical hardness, softness, electrophilicity index and density of states (DOS) are calculated.

These results may be useful not only to understand adsorption capability of BNNTs, but also to develop BNNT-based sensors in environment. Calculated data for the electronic density of states and the electronic charge densities indicate that the doping of C atom not only improves the electronic transport property of the BNNT but also induces magnetism in the odd carbon doped SW-BNNTs. In addition, doping SW-BNNTs with C is expected to be an available strategy for improving the properties of BNNTs, and C doped SW-BNNT is expected to be a potential resource for detecting the presence of NO and, in turn, to develop BNNT-based sensors in environment.

Computational details

All geometry optimization calculations were performed using the B3LYP hybrid functional^{52,53} and 6-31+G(d) basis set as implemented in the computational program packages.^{54,55} Furthermore, single-point energies have been obtained at the M06-2X/6-31+G(d) level .

We have investigated the effects of SW defect and C-doping in different sites of SW defect region on the electronic and structural properties of (6, 0) zigzag single-walled BNNT. For this purpose a single-walled BNNT with 36 B and 36 N atoms and the average length about 11.39 Å was used to model the (6,0) BNNTs. Both ends of the BNNT segment were capped with H atoms to saturate dangling bonds. The formation energies of the C-doped SW defective BNNTs were estimated using equation (1) given below:

$$E_{form} = E_d + (a + b)E_{B \text{ or } N} - mE_C - E_p \quad (1)$$

where E_d is the calculated total energy of BNNT containing defects, $E_{B \text{ or } N}$ is the total energy of host boron or nitrogen atoms removed from the nanotube, E_C is the total energy calculated for the atomic carbon, E_P stands for the total energy calculated for the pristine BNNT and a , b , and m are the number of B, N, and C atoms, respectively. The band gap is obtained from the difference between the orbital energies of the LUMO (conduction band minimum) and the HOMO (valence band maximum). To plot the density of states (DOS), we were used the Multiwfn software.⁵⁶

Global reactivity descriptors measure the overall reactivity of a molecule. They are associated with the overall reactivity of the molecule and do not contain any information about regioselectivity. Some of descriptors are chemical potential, chemical hardness, global softness etc. Chemical potential plays an especial important role in semiconductor physics⁵⁷ and their reactivity in chemistry. The DFT-based reactivity descriptors are good prediction tools for studying reactivity especially in probing the regiochemistry of different types of chemical reactions.⁵⁸⁻⁶⁰

The relation of chemical potential (μ) and the electronegativity (χ)^{61,62} can be written as follows:

$$\mu = -\chi = -\frac{1}{2}(I + A) \quad (2)$$

The global chemical hardness (η) is defined as⁶³

$$\eta = \frac{1}{2}(I - A) \quad (3)$$

Where I and A are the first ionization energy and electron affinity, respectively. The chemical meaning of the word “hardness” is resistance of the chemical potential to change in the number of electrons.

In the finite different approximation, the ionization energy and electron affinity can be replaced by the E_{HOMO} and E_{LUMO} , respectively, using Koopmans' theorem.⁶⁴

$$\mu = -\chi = \frac{1}{2}(E_{HUMO} + E_{LUMO}) \quad (4)$$

$$\eta = \frac{1}{2}(E_{LUMO} - E_{HOMO}) \quad (5)$$

The electrophilicity index (ω),⁶⁵ which measures the capacity of an electrophile to accept the maximal number of electrons in a neighboring reservoir of electron sea, is defined according to the following equation

$$\omega = \frac{\mu^2}{2\eta} \quad (6)$$

The chemical softness (S) is defined as following equation

$$S = \frac{1}{\eta} \quad (7)$$

An ONIOM methodology⁶⁶ is used to study the adsorption of NO gas on the C-doped SW-BNNTs. ONIOM approach has clear advantages for modeling interactions involving nanostructures.⁶⁷⁻⁶⁹ In this approach, the full system is divided into a reactive part, which is treated at an appropriately high level of theory, while the remainder of the system is included at a less expensive lower level of theory. This ensures an appropriately high level of accuracy for the reactive part of the system, while reducing the computational cost by only calculating this smaller part with the expensive method. Atoms in a lower level bound to an atom in a higher level are replaced by hydrogen atoms during the higher-level part of the ONIOM calculation. In the ONIOM methodology used in this work, small part of the nanotube including the NO molecule and the atoms of SW region was treated using the M06-2X functional together with the 6-31++G(d,p) basis set, while rest of the system (low theoretical level) was treated using the same method and STO-6G basis set. In addition, single point calculations were performed on the optimized structures at the M06-2X/6-31++G(d,p) level of theory to obtain the most reliable energies. To confirm the results of the ONIOM model, we also carried out the full optimization at M06-2X/6-31++G(d,p) level of theory and in turn calculation of adsorption energy for 2C-doped SW-BNNT complexes.

3. Results and discussions

The nine kinds of C-doped SW-BNNT are investigated. The calculated models are shown in Fig. 1. The studied BNNTs are pristine $B_{36}N_{36}H_{12}$ (**D**), SW-BNNT $B_{36}N_{36}H_{12}$ (**E**) and C-doped SW- $B_{36}N_{35}CH_{12}$ (**F_N**), SW- $B_{35}N_{36}CH_{12}$ (**G_B**), SW- $B_{35}N_{35}C_2H_{12}$ (**H₁₃**), SW- $B_{36}N_{34}C_2H_{12}$ (**I₃₄**), SW- $B_{34}N_{36}C_2H_{12}$ (**J₄₅**), SW- $B_{36}N_{33}C_3H_{12}$ (**K₁₂₃**), SW- $B_{35}N_{34}C_3H_{12}$ (**L₁₃₄**), SW- $B_{34}N_{35}C_3H_{12}$ (**M₃₄₅**) and SW- $B_{33}N_{36}C_3H_{12}$ (**N₄₅₆**). We have used symbols **G_B**, **F_N**, **H₁₃**, **I₃₄**, **J₄₅**, **K₁₂₃**, **L₁₃₄**, **M₃₄₅** and **N₄₅₆** for C-doped SW-BNNTs C_B , C_N , C_{2N} , C_{NB} , C_{2B} , C_{3N} , C_{2N1B} , C_{1N2B} and C_{3B} , respectively.

3. 1. 1C-doped (6,0) SW defective BNNTs

In the one C-doped SW-BNNTs, one N or B atom of the vertical B-N bond in the SW defect region was substituted by one carbon atom (denoted as **F_N** and **G_B**, respectively). The bond length values of L_1 to L_{11} bonds are listed in Table 1. Due to the presence of unfavorable electronic interactions N-N and B-B, stability of SW-BNNTs decreases with respect to the pristine BNNT. The homonuclear N-N (1.469 Å) and B-B (1.711 Å) bonds are longer than corresponding bonds in C-doped SW-BNNTs (1.419 Å in **F_N** and 1.533 Å in **G_B**). The L_6 bond length is 1.438 Å, 1.540 Å and 1.427 Å in the SW-BNNT (**E**), **F_N** and **G_B** models, respectively, indicating that vertical B-C bond is longer than vertical B-N and C-N bonds. Therefore, substitution of C atom increases and decreases L_6 bond in **F_N** and **G_B** models, respectively. Since the atomic radius of C atom is larger than N and smaller than B atom, substitution of N by C in the vertical B-N bond increases L_6 bond. The two other bond lengths between N3 atom and neighbouring atoms (L_1 and L_5) in SW-BNNT is 1.469 and 1.495 Å that change to 1.419 and 1.595 Å in **F_N** nanotube, respectively. Besides, L_7 (1.711 Å) and L_{11} (1.468 Å) bonds around the B4 atom decrease to 1.553 and 1.431 Å upon substitution of B by C atom in **G_B** nanostructure, respectively. This reduction can be attributed to lower

atomic radius of C atom with respect to the B one. In general, the change in bond lengths upon C doping into the N atom in \mathbf{F}_N nanostructure is greater than B atom in \mathbf{G}_B one.

Table 2, presents the sum of three bond angles around the six situations of structures given in Fig. 1. Sum of the three bond angles is 342.6° around the third situation in \mathbf{E} model and 345.8° and 336.0° in \mathbf{F}_N and \mathbf{G}_B models, respectively. Moreover, it is 351.8° and 353.3° around the fourth site in \mathbf{E} and \mathbf{G}_B models, respectively. These changes show that the C doped atoms increase the sum of three mentioned bond angles. The presence of lone pair in N atom decreases the bond angle between the bonding pair of electrons and the sum of three bond angles. There is a simple interpretation; the carbon atom in \mathbf{F} model is a radical that has unpaired valence electrons or an open electron shell, therefore radical carbon decrease bond angles less than lone pair of nitrogen.

Li et al. reported that the defect formation energies of SW- BNNTs depend on the tube radii⁷⁰. They have calculated defect formation energies in a series of zigzag (n,0) (n = 7, 8, 10, 12) SW-BNNTs. They have shown that defect formation energy increases with increasing tube diameters. The calculated defect formation energies of BNNTs are given in Table 3. The formation energy of SW-BNNT (\mathbf{E}) is greater than pristine BNNT (\mathbf{D}) by 3.95 eV, indicating that the formation of SW defect destabilize BNNT. Our calculated defect formation energy (3.95 eV using B3LYP and 4.21 eV using M06-2X) is in good agreement with that of reported by Li et al.⁷⁰ for (7,0) SW-BNNT (4.5 eV). The presence of pentagon and heptagon rings having B-B and N-N bonds violates the $[4n + 2]$ aromatic rule and causes the undoped SW-BNNTs to be less stable electronically compared with the perfect hexagonal structures with six π electrons. The calculated formation energies of \mathbf{F}_N and \mathbf{G}_B models are 4.06 eV and 3.41 eV, respectively, indicating a greater probability for the C atom to replace the boron atom than the nitrogen atom. Formation energy of \mathbf{G}_B is approximately 0.5 eV and 0.6 eV lower than undoped SW-BNNT and \mathbf{F}_N , respectively. Therefore, \mathbf{G}_B model is appeared to be

more energetically stable than **E** and **F_N** models, in good agreement with the calculated structural parameters. However, the higher positive values of formation energies in the C substitution also show the low probability of finding B and N defects in the SW-BNNT. These computational results are consistent with the observations which were obtained from formation energy of native defects in BN nanotubes.⁷¹

The defect formation energies calculated using highly parameterized empirical M06-2X functional, that implicitly accounts for “medium-range” electron correlation, are greater than B3LYP one. In spite of the greater formation energies calculated using M06-2X functional; the order of the stability of BNNTs is same using both methods.

The electronic energies of NTs are studied for further investigation of effect of one carbon-doping in (6,0) SW-BNNTs. The energies of the highest occupied molecular orbital (HOMO), the lowest unoccupied molecular orbital (LUMO) and the energy gap between LUMO and HOMO are tabulated in Table 3. The role of doping atom C (as impurity) can be explained from comparison of HOMO energies. As can be seen in Table 3, HOMO energy of undoped **E** NT is -6.52 eV that increases to -5.71 and -4.46 eV in C-doped **F_N** and **G_B** NTs, respectively. This makes the **G_B** NT a good electron donor than undoped BNNT and **F_N** NT. In addition, C-doping slightly increases LUMO energy in **F_N** and decreases in **G_B** as compared with that of **E** NT. The greater increase in HOMO energy level makes the donor level near the conducting band and in turn decreases the band gap.

The band gaps of CNTs are small (from 0.2 to 2.0 eV), so CNTs are either metallic or semi-conductive, while band gaps of pure BNNTs are much bigger (of 5.0–6.0 eV width), so they are wide-gap semiconductor or insulator. The number of electrons excited thermally is proportional to $e^{(-E_{\text{gap}}/2RT)}$. Increasing the temperature or decreasing the band gap energy leads to higher conductivity for an intrinsic semiconductor. According to our calculations, the band gap energy of the **D** and **E** NTs are 4.3 and 4.5 eV, respectively. The calculated band gap

energy of the F_N and G_B is 3.5 and 2.2 eV, respectively, indicating the band gap is decreased on going from pristine and SW-BNNTs to one carbon doped SW-BNNT. The substituting C for B atom decreases band gap more than that of substituting F for N atom. This makes G_B a wide-gap semiconductor. There is a simple interpretation for lower band gap of G_B (C substitution for B atom): The C atom (donor impurity atom) without the donor electron (fourth valence electron) is positively charged. At very low temperatures, the donor electron is bound to the C atom. However, by intuition, it should seem clear that the energy required to elevate the donor electron into the conduction band is considerably less than that for the electrons involved in the covalent bonding.

Calculated results show that one C-doped BNNTs are intermediate in energy band gap between CNTs and BNNTs, and present characters of semiconductor. In this way, BNNTs can also be transformed from insulators to semiconductor through intentional C doping. These results are in complete agreement with the early experimental and theoretical results.^{29,72} The band gaps of all models obtained using M06-2X are qualitatively similar to those calculated by using B3LYP approach.

To gain deeper insights into the electronic structure of the C-doped SW-BNNTs, we further calculated their density of states (DOS). The DOS for D , E , F_N , and G_B nanostructures are shown in Fig. 2. The energy difference between HOMO and LUMO orbitals makes the D model an insulator with a wide band gap. The HOMO-LUMO gap of the E model compared with the D model is slightly narrowed because of the SW defect.⁷³ The DOS curves are changed by the B or N substitutions for C in vertical B-N bond of SW-BNNT. Carbon atom has one less (or more) electron than B (or N) atom. Therefore, when a B (or N) atom is substituted by a carbon atom, an electron (or hole) is introduced into the relevant structure. This extra valence electron (or hole) provides defect levels within the HOMO-LUMO gap of (6,0) SW-BNNT.^{74,75,76} Accordingly, the band gap of F_N model on

top of valence band (VB) consists of acceptor level and the \mathbf{G}_B model at the bottom of conduction band (CB) consists of donor level. As can be seen in Fig. 4, DOS curves of C-doped NTs are different from the undoped NTs (\mathbf{D} and \mathbf{E}). It is clear that C impurity has a significant contribution to the DOS appeared in band gap. For the \mathbf{G}_B model, there is a peak in the middle of band gap, and the DOS at Fermi level is non-zero indicating that electrons will be able to transfer from donor level to conducting band. The C doping in \mathbf{F}_N NT provides an empty level to the band gap. For \mathbf{F}_N model, there is a peak near the valence band and the DOS is also non-zero at Fermi level. Electrons in \mathbf{F}_N model can be more easily excited from filled band to acceptor level than to the conducting band, so that excitation from filled band to acceptor level yields an electron hole. This formed hole leads to the conductivity of P-type semiconductor.^{13,76,77}

As we know, the boron or nitrogen atoms in un-doped BNNTs are connected to three neighbor atoms by three single bonds, therefore all electrons in a BN hexagonal structure should be paired and the structure should not present spin polarization. Therefore, ground states of the pure (6,0) SW-BNNT is nonmagnetic while the isolated NO has clear magnetism for the unpaired electron. However, present of a carbon atom in the \mathbf{F}_N and \mathbf{G}_B structures and three C atoms in \mathbf{K}_{123} , \mathbf{L}_{134} , \mathbf{M}_{345} and \mathbf{N}_{456} , ones causes the appearing of an unpaired electron and therefore a net spin polarization. The p_z orbital is isolated with one electron occupation leads to a spin moment. Therefore, C doping results in the spin polarization and induces spontaneous magnetization. It is possible to deduce that a C-doped SW-BNNT with odd numbers of carbon atoms will always present unpaired spins while, for even numbers, it would display paired spins. To explore whether C doping can induce the spin polarization, the spin DOSs of the most stable \mathbf{F}_N and \mathbf{G}_B C-doped SW-BNNTs are calculated and shown in Fig. 2b. From this figure, it can be found that new local states are appeared and spin-up and spin-down DOSs are different in band gap region, indicating that C-doping results in the

spin polarization and induces spontaneous magnetization. Carbon atom has one less (or more) electron than N (or B) atom. Therefore, when a B (or N) atoms is substituted by a carbon atom, an electron (or hole) is introduced into related structures, accompanied by the formation of defect levels within the HOMO–LUMO gap.

As the computational results revealed, the band gap energy of C-doping SW-BNNTs was smaller than undoping one. Therefore the conductivity of SW-BNNTs may easily be modified by introducing C doping into their structures and can be converted to semiconductors. This defect affects the global descriptors and electric dipole moments. The calculated amounts of μ , η , S , ω and dipole moment (Q) are tabulated in Table 4. It can be observed that hard molecules have a large E_g and soft molecules have a small one. It should be mentioned that the soft molecules with a small gap will be more polarizable than the hard ones. Chemical potential of the electrons has much the same significance as the chemical potential in the classical thermodynamics of macroscopic systems. In the Hohenberg-Kohn density functional theory of the ground state, chemical potential is defined as the partial derivative of the systems energy with respect to the number of electrons at constant external potential v : $\mu = \left(\frac{\partial E}{\partial N} \right)_v$. The physical meaning of chemical potential in DFT is to measure the escaping tendency of an electron cloud. It is constant in three dimensional space for the ground state of an atom, molecule or solid and equals the slope of E versus N curve at constant external potential.⁴¹ As can be seen, μ for all NTs is negative. The absolute values of chemical potential, $|\mu|$, of **E** and **G_B** models are smaller than their own corresponding models (**D** and **F_N**), respectively. For **D** to **G_B** models, the lowest absolute value of chemical potential belongs to **G_B** model (3.36 eV). Thus, **D** and, **E** and **F_N** NTs have much steeper slope than **G_B**. The lowest $|\mu|$ means that there is a little accepting tendency of an electron for **G_B**. The hardness index, η , is positive for All NTs, indicating that the charge transfer is an

energetically favorable process. **D** and **E** NTs have a larger hardness than the **F_N** and **G_B** doped NTs, indicating that in gas phase the **D** and **E** NTs should be more stable than the **F_N** and **G_B**. There is a correlation between chemical potential and hardness index. Among the mentioned NTs, the lowest η and $|\mu|$, is corresponds to doped **G_B** NT. Therefore, **G_B** with lowest η is less stable than others. In contrast to η , as expected, the softness index S increases on going from **D** (0.44 eV^{-1}) to **G_B** (0.91 eV^{-1}). Softness index is proportional to the polarizability of the system. The hardness can be thought of as a resistance to charge transfer, while the softness measures the ease of transfer. The thermodynamic aspect of ω helps to explain, qualitatively, favorable product formation, because ω is positive for all NTs, charge transfer is an energetically favorable process. The greater electrophilicity index of **G_B** doped NT shows that the energy lowering of NT (stabilization energy) due to maximal electron flow between donor and acceptor is bigger than others. Since **G_B** doped NT possesses a bigger electrophilicity index, it has better capability to accept electrons than the others. The rate of the reaction can be associated with the global electrophilicity value. If the substrate is an electron acceptor then higher ω value will favor the reaction and for electron donor substrate naturally the lower ω value will favor the reaction leading to the lower activation energy. The maximum value of dipole moment, Q , is related to **F_N** model (7.20 Debye).

3. 2. Tow carbon-doping in (6,0) SW defective BNNTs

As mentioned above, the presence of homoelemental N-N and B-B bonds unstable the SW-BNNT. Two substitutional carbon atoms in C-C doping of SW-BNNTs prohibit the formation of N-N and B-B bonds. The vertical N-B bond as well as N-N and B-B bonds was chosen in SW-BNNT for substitution of C-C pair atoms. The C-C doped nanostructures **H₁₃**, **I₃₄** and **J₄₅** are shown in Fig. 1. The calculated C-C bond lengths are 1.380, 1.370 and 1.382 Å in the **H₁₃**, **I₃₄** and **J₄₅** models, respectively, indicating that the vertical C-C bond is shorter than two slanted ones. The C-C bond length in all **H₁₃**, **I₃₄** and **J₄₅** structures is shorter than

C–N, B–N and B–C bond lengths; all the B–C bond lengths are longer than the C–N and B–N bond lengths. Wan et al.⁷² have reported similar results on (3,2) BNNTs. After C–C bonds, the heteroatom C–N bond in **I**₃₄ (1.446 Å) and **J**₄₅ (1.428 Å) and heteroatom B–N bond in **H**₁₃ (1.470 Å) are smallest bonds. The B–B (1.721 Å) and N–N (1.488 Å) bonds in **H**₁₃ and **J**₄₅ are longer than that of undoped SW-BNNT (1.711 Å and 1.469 Å). The longest bond in defective region of **H**₁₃ and **J**₄₅ models is L₇ (B–B) and L₅ (B–N), respectively. The change in bond lengths upon substitution of C atoms are due to the order of covalent radius of anions is B > C > N. Sum of three bond angles around 1 to 6 sites of the **H**₁₃, **I**₃₄ and **J**₄₅ models given in Fig. 1 are listed in Table 2. After C atoms doped, the difference between the maximum and the minimum of bond angles increases. This difference for undoped SW-BNNT, **H**₁₃, **I**₃₄ and **J**₄₅ models is 17.5, 21.0, 20.2 and 38.2°, respectively. The sum of three bond angles around the C atom in central 7-7 ring fusion (vertical L₆ bond) of **H**₁₃, **I**₃₄ and **J**₄₅ NTs is 347.2, 350.2 and 359.3°, respectively. Therefore, when BNNTs have an impurity in SW defect region, the local geometry will change around the impurity.

The stability of 2C-doped structures is evaluated through calculating the defect formation energy given in Table 3. As can be seen, the defect formation energy for **H**₁₃, **I**₃₄ and **J**₄₅ NTs is 4.33, 0.71 and 2.27 eV, respectively, indicating that its value for NT including vertical C–C bond is smallest. Defect formation energy of **I**₃₄ is approximately 3.2 eV, 3.6 eV and 1.36 eV lower than undoped SW-BNNT, **H**₁₃, and **J**₄₅, respectively, in good agreement with the results given in.³⁴ Consequently, substitution of vertical B–N bond in defect region by C–C bond leads to a nanostructure that is more stable than other 2C-doped SW-BNNTs. The smallest defect formation energy is observed for **I**₃₄ NT in which has smallest C–C bond. It should be mentioned that unfavored B–B and N–N bonds is removed upon substitution of C–C bond in **I**₃₄ NT. Therefore, **I**₃₄ model is most favorable among all of the 2C-doped models.

The high defect formation energy in \mathbf{H}_{13} and \mathbf{J}_{45} NTs is due to the presence of one unstable B-B and N-N bond.

We have also used the high parameterized functional M06-2X for calculation of defect formation energy. The results in Table 3 show that defect formation energies calculated using M06-2X functional are greater than B3LYP functional.

The electronic properties of 2C-doped (6,0) SW-BNNT are calculated. Moreover the HOMO-LUMO gaps for \mathbf{H}_{13} , \mathbf{I}_{34} and \mathbf{J}_{45} models are calculated that the results are shown in Table 3. According to the results, the band gap of the 2C-doped SW-BNNTs changes from 2.9 eV to 3.6 eV at B3LYP/6-31+G(d) level. These values are smaller than that of pristine BNNT (4.50 eV) and SW-BNNT (4.27 eV). The results show that the energy gap depends on the 2C-doped positions.⁴⁹ In comparison with the band gap of \mathbf{H}_{13} (3.58 eV) and \mathbf{J}_{45} (2.86 eV) models, the energy gap in the most stable NT \mathbf{I}_{34} is greater (3.86 eV). For pristine BNNT, SW-BNNT and 2C-doped SW-BNNTs, the order of energy gap is pristine > SW-BNNT > \mathbf{I}_{34} > \mathbf{H}_{13} > \mathbf{J}_{45} . The presence of carbon atoms in 2C-doped SW-BNNTs leads to decrease of band gap. The decrease in the band gap is 0.69, 0.41 and 1.41 eV for \mathbf{H}_{13} , \mathbf{I}_{34} and \mathbf{J}_{45} models, respectively. The band gaps values calculated using M06-2X functional are noticeably overestimated as compared to those of obtained using the B3LYP one.

The total and partial DOS of \mathbf{H}_{13} , \mathbf{I}_{34} and \mathbf{J}_{45} models are shown in Fig. 3. According to these curves, the band gaps of 2C-doped SW-BNNTs depend on situations where carbon atoms are replaced. In \mathbf{H}_{13} NT, two N atoms are substituted with two C atoms so that each carbon atom is connected to one C atom and two B atoms. In contrast to \mathbf{E} NT, DOS curve of \mathbf{H}_{13} has one impurity state in which is close to the unoccupied molecular orbital as shown in Fig. 3. The Fermi level in \mathbf{I}_{34} moves toward more positive energy compared with Fermi level of \mathbf{E} model. DOS curve of \mathbf{J}_{45} shows a bulge near the valence bond in HOMO-LUMO gap that is created by carbon impurity.

The calculated values of μ , η , S , ω , and Q for **H₁₃**, **I₃₄** and **J₄₅** models are reported in Table 4. As can be seen, the μ for **J₄₅** model is (-3.70 eV) greater than those of **H₁₃** and **I₃₄** models. In addition, the hardest structure corresponds to **I** model, so this model with a large η is less polarizable than **I₃₄** and **J₄₅** models. The values of S , ω and Q for **I₃₄** model are smaller than those of **H₁₃** and **J₄₅** ones. The electrophilicity index ω determines what extent partial electron transfer contributes to the lowering of the total binding energy by maximal flow of electrons. As a result, tendency of **I₃₄** doped NT to react with a nucleophile is smaller than others. In other words, low value of ω for **I₃₄** compared with **H₁₃** and **J₄₅** makes it little more likely for **I₃₄** to react with a nucleophile than others.

3. 3. Three carbon-doping in (6,0) SW defective BNNTs.

Different boron and nitrogen atoms of the pentagon pair of SW-BNNTs are doped with three carbon atoms. The defective nanostructures are modeled by using **K₁₂₃**, **L₁₃₄**, **M₃₄₅** and **N**, as it is shown in Fig. 1. The **K₁₂₃** and **N₄₅₆** models have an unfavorable homoelemental N-N and B-B bond, respectively. In addition, four C-B bonds and one C-C bond in structure of **K₁₂₃** and four C-N bonds and one C-C bond in structure of **N₄₅₆** is observed. In **L₁₃₄**, one B and two N atoms in SW defect region are substituted by three C atoms so that two neighbouring C-C bonds are formed between them. In **M₃₄₅**, one N and two B atoms in SW defect region are replaced by three C atoms so that two C-C bonds are formed between them. However, 3C-doped **L₁₃₄** and **M₃₄₅** have no unfavorable homoelemental B-B and N-N bonds.

The bond length values for these models are also shown in Table 1. The only C-C bond in **K₁₂₃** (1.393 Å) and **N₄₅₆** (1.375 Å) is shorter than other bonds. Besides, L_7 (B-B) bond length in **K₁₂₃** model and L_5 (N3-B) bond length in **N₄₅₆** model are longer than other bonds. There is two C-C bonds in **L₁₃₄** ($L_1 = 1.430$ Å and $L_6 = 1.405$ Å) and **M₃₄₅** ($L_6 = 1.409$ Å and $L_7 = 1.439$ Å) models so that their bond lengths are shorter than other bonds in SW defect

region. The C–C bond at the 7-7 ring fusion (L_6) is shorter than C–C bond at the 5-7 ring fusion (L_7 in \mathbf{M}_{345} and L_1 in \mathbf{L}_{134}). Besides, L_1 in \mathbf{L}_{134} is shorter than L_7 in \mathbf{M}_{345} .

According to the results given in Table 2, the sum of three bond angles around the C atom in \mathbf{K}_{123} , \mathbf{L}_{234} , \mathbf{M}_{345} , and \mathbf{N}_{456} models change compared to those of similar positions in \mathbf{E} model. These changes are more sensible when only either N–N bond or B–B bond is replaced by one C–C bond. For example, the sum of three bond angles around the 4, 5 and 6 positions in the \mathbf{N}_{456} model are 359.6° , 360° , and 339.5° respectively, whereas the sum of three bond angles around these points in \mathbf{E} model are 351.8° , 356.3° , and 357.1° respectively. For \mathbf{L}_{134} and \mathbf{M}_{345} models, sum of the bond angles around the C atom at the 5-7 ring fusion (i.e. 3 and 4 in \mathbf{L}_{134} and 4 and 5 in \mathbf{M}_{345}) are greater than those of the 7-7 ring fusion.

Based on results given in Table 3, the maximum value of defect formation energy belongs to the \mathbf{K}_{123} model in which the three nitrogen atoms in 1, 2, and 3 sites are replaced by three carbon atoms. After \mathbf{K}_{123} , defect formation energy for \mathbf{N}_{456} model, in which B atoms are substituted with C atoms, is greater than others. The minimum value of defect formation energy corresponds to the \mathbf{M}_{345} model in which one nitrogen atom and two boron atoms are replaced by three carbon atoms in third, fourth, and fifth sites. Hence, \mathbf{M}_{345} model is the most stable structure. The stability of 3C-doped SW-BNNTs is arranged as $\mathbf{K}_{123} < \mathbf{N}_{456} < \mathbf{L}_{134} < \mathbf{M}_{345}$. From these results, it can be proposed that the pairs of neighbouring C–C defects lead to lower formation energies than configurations where these defects are spatially separated, due to the charge compensation between them. As can be seen in Table 3, defect formation energies obtained by M06-2X functional are greater than B3LYP one.

The effects of three carbon doping of SW-BNNT on the electronic properties of (6,0) SW-BNNTs are also investigated. The results are shown in Table 3. The electrical conductivity of a semiconductor can be greatly increased by doping with impurities. The value of band gap energy of 3C-doped SW-BNNTs is arranged as $\mathbf{L}_{134} > \mathbf{K}_{123} > \mathbf{M}_{345} > \mathbf{N}_{456}$.

The maximum value of band gap energy belongs to the L_{134} model in which two N and one B atoms are replaced with three C atoms and the minimum value belongs to the N_{456} model that three B atoms are substituted with three C atoms. From the difference in band gaps, it can be concluded that the C substituting B are narrow-gap semiconductor, while C substituting N are wide-gap semiconductor. In other words, decrease in B atoms of SW defect region is accompanied with decrease in band gap energy. These results lead us to suggest that the SW-BNNTs can be transformed from electrical insulators or wide band gap semiconductors to narrow-band gap semiconductors or a conductor. Also, such nanostructures exhibit tunable semiconductivity. In addition, minimizing band gap energy in nanostructures so as to harvest more sunlight is one of the critical factors towards enabling high-efficiency solar cells. Therefore, from these results it can be predicted that the C_B -doped SW-BNNTs with lower band gap energy can be used to improve solar cell efficiency.

The effect of 3C-doping on electronic properties of SW-BNNT can be explained from comparison of HOMO and LUMO energies. The results show that the value of HOMO energy depends on location of carbon impurity. As can be seen in Table 3, HOMO energy of N_{456} NT (-3.98 eV) (three B atoms are replaced by three C atoms) is greater than others and for K_{123} (-6.39 eV) (three N atoms are replaced by three C atoms) is smaller than others. The HOMO energy values of L_{134} and M_{345} lie between N_{456} and K_{123} . Therefore, doped BNNTs including two neighboring C atoms and one separated C atom have greatest and lowest HOMO energy. The LUMO energy of 3C-doped NTs is ordered as $L_{134} \sim M_{345} > N_{456} > K_{123}$. The greater increase in HOMO energy level of N_{456} makes the donor level moves near the conducting band and in turn decreases the band gap. The results show that the presence of three neighboring C atoms causes the energy of LUMO in M_{345} and N_{456} to be greater than others.

DOS curves of 3C-doped BNNTs are shown in Fig. 4. As illustrated in this figure, the DOS curves are sensitive to the position of dopant atoms. As expected, DOS curve in \mathbf{K}_{123} model (as a P-type semiconductor) and \mathbf{L}_{134} models has one bulge near the conducting and valence band, respectively. In addition, position and electron density of Fermi level are different in these two models. Compared with the \mathbf{K}_{123} , the Fermi level in \mathbf{L}_{134} model is closer to the middle of band gap. The electron density in Fermi level is greater for \mathbf{K}_{123} than \mathbf{L}_{134} . The formation of new peaks and presence of Fermi level at the middle of the band gap of \mathbf{M}_{345} and \mathbf{N}_{456} SW-BNNTs is predicted to be the main doping effect on the greater conductivity of these NTs. The mid gap states positioned inside the band gap of 3C-doping NTs make them attractive for band gap engineering in, for example, photocatalytic applications.

The global quantities μ , η , S , ω , and Q for 3C-doped BNNTs are given in Table 4. The greatest value μ is (-3.15 eV) which it belongs to the \mathbf{N}_{456} doped NT in which three B atoms are replaced by three C atoms. Therefore, escaping tendency of an electron cloud in \mathbf{N}_{456} is greater than others 3C-doped BNNTs. The μ value of \mathbf{M}_{345} with lowest defect formation energy is greater than those of \mathbf{L}_{134} and \mathbf{K}_{123} and smaller than \mathbf{N}_{456} . Therefore, after \mathbf{N}_{456} tendency of electron to escape from 3C-doped NT is greater in \mathbf{M}_{345} than others. From values of η and S , it can be estimated that the resistance to charge transfer in \mathbf{N}_{456} and \mathbf{M}_{345} is smaller than others 3C-doped NTs. Among the 3C-doped NTs, greatest ω values correspond to the \mathbf{K}_{123} (7.23 eV) and \mathbf{N}_{456} (6.05 eV) including the two neighboring C atoms and one separated C atom. Since \mathbf{K}_{123} and \mathbf{N}_{456} doped NT possesses a bigger electrophilicity index, they have better capability to accept electrons than the others. The results show that the dipole moment of \mathbf{N}_{456} is smaller than others.

3. 4 General comparison or General review

Comparison of structural parameters in C-doped NTs shows that all the C–C bond lengths are shorter than the C–N, B–N and B–C bond lengths. The B–C bond lengths at the different situations of the SW-BNNTs are longer than the C–N and B–N bond lengths. These results are in good agreement with the previous work.^{35,50}

According to the obtained results, defect formation energies obtained using two B3LYP and M06-2X functionals are arranged as: $I_{34} < M_{345} < L_{134} < J_{45} < N_{456} < G_B < E < F_N < H_{13} < K_{123}$. As can be seen, defect formation energy for doped SW-BNNTs in which two B and one N atom at the central 7-7 ring fusion (vertical bond) are substituted with C (I_{34} , M_{345} and L_{134}) is smaller than others. Therefore, formation of these types doped NTs are energetically most favorable. In contrast, doped NTs in which is formed by substitution of N atom by C atom (F_N , H_{13} and K_{123}) have greatest formation energy. Among the C-doped NTs, the lowest defect formation energy belongs to the I_{34} (0.71 eV) and M_{345} (0.75 eV) and greatest value corresponds to K_{123} (6.92 eV) which is formed by substitution of three carbon atoms with three nitrogen atoms in pentagon ring of SW defect region.

The band gap energies of F_N to N_{456} models depends on the number of B or N atoms which are substituted by C atoms as well as the positions in which they are stayed. Generally, decrease in band gap is more evident when the boron atoms are replaced by carbon atoms (G_B , N_{456} and M_{345}). Accordingly, band gap energies of studied NTs are ordered as: $N_{456} < M_{345} < G_B < J_{45} < K_{123} < L_{134} < F_N < H_{13} < I_{34} < E < D$. As a result, N_{456} NT that is formed by substitution of three B atoms with three C atoms has smallest band gap energy and in turn more conductivity.

Comparison of global descriptors shows that the N_{456} BNNTs with a narrow band gap have greatest value of μ , S and ω and smallest value of η , indicating that the reactivity and conductivity properties of this NT is greater than others. Based on the Pearson's maximum hardness principle,⁷⁸ which states that the minimum energy structure has the maximum

chemical hardness and the energy gap, the I_{34} C-doped SW-BNNT is the most stable structure among the C-doped nanostructures. There is a correlation between S and band gap energy of studied BNNTs. As can be seen in Tables 3 and 4, increase in S index is accompanied with decrease in band gap. According to the DOS curves of D to N_{456} models, the energy of Fermi levels increases (decreases) when B (N) atoms are substituted with the carbon atoms in the (6,0) SW-BNNT.

3.5. Adsorption of a single NO molecule on C-doped SW-BNNT

The various possibilities of NO adsorption on the outer surface of C-, 2C- and 3C-doped SW-BNNTs were explored to achieve the intuitive understanding of the adsorption process. The NO monomer can be attached to BNNT through the N-atom (N_{ad}), O-atom (O_{ad}), and N-O ($N_{ad}O_{ad}$) bond.

For 1C-doped SW-BNNTs, four chemisorbed F_{ON} , F_{NO} , G_{ON} and G_{NO} complexes were found on potential energy surface and selected structural parameters are given in Fig. 5. The ON (N-down) and NO (O-down) symbols represent the different direction of NO toward the tube axis. As can be observed, NO molecule is located on top of the NT and interacts with the C atom of NT via both O and N atoms (in F_{NO}), O atom (in G_{ON}) and N atom (in G_{NO} and F_{NO}).

The HOMO (E_H), LUMO (E_L), and band gap energies (E_g) of free H-N nanotubes calculated at M06-2X/6-31++(d,p) level are given in Table 5. Besides, electronic adsorption energies (AEs), HOMO, LUMO and band gap energies obtained at M06-2X/6-31++(d,p) level for complexed BNNTs are given in Table 6.

The calculated AEs of F_{ON} , F_{NO} , G_{ON} and G_{NO} , are -9.963, -31.29, 6.96 and -33.62 kcal/mol, respectively. The results indicate that the adsorption process of NO on 1C-doped SW-BNNTs (F_{ON} , F_{NO} and G_{NO}) is energetically favorable. Comparison of AEs shows that the F_{NO} and G_{NO} complexes, in which N atom of NO is bonded to C one, are most stable

ones. Thus, the best adsorption site for NO gas molecule in 1C-doped SW-BNNTs found to be above the C substitution for B site. After F_{NO} and G_{NO} complexes, F_{ON} complex is energetically favorable to be formed. The AE is positive for G_{ON} complex in which O atom of NO is connected to C one, indicating that this site is not energetically suitable for adsorption.

For 2C-doped SW-BNNTs, eight chemisorbed H_{ON} , H_{NO} , I_{ON} , I_{NO} , $I_{NO(N)}$, $I_{NO(O)}$, J_{ON} and J_{NO} NO-SW-BNNT complexes were optimized at ONIOM(M06-2X/6-31++(d,p):M06-2X/STO-6G) level and selected structural parameters are given in Fig. 5. As can be seen, NO molecule in most complexes is located on top of the NT and interacts with the C-C bond of NT via both O and N atoms, resulting in the formation of a four-membered ring. In complexes L_{NO-1} , L_{NO-2} , M_{NO-2} , $I_{NO(N)}$ and $I_{NO(O)}$, NO molecules are connected with the C atoms through the N and or O atoms.

The AEs calculated for H_{ON} , H_{NO} , I_{ON} , I_{NO} , $I_{NO(N)}$, $I_{NO(O)}$, J_{ON} , J_{NO} , K_{ON} , K_{NO} , L_{NO-1} , L_{NO-2} , L_{ON-1} , L_{ON-2} , M_{NO-1} , M_{NO-2} , M_{ON-1} , M_{ON-2} , N_{ON} , N_{NO} complexes are 4.55, 5.11, -0.46, -0.47, 2.05, 62.10, -0.35, -10.35, -11.53, -29.59, -5.01, -29.36, 17.98, 24.53, -24.29, -29.39, 1.16, 11.78, -25.15, -31.72 and -5.61 kcal/mol, respectively. The results indicate that the adsorption process of NO on 2C-doped SW-BNNTs I_{ON} , I_{NO} , J_{ON} and J_{NO} is energetically favorable. Comparison of AEs shows that the J_{ON} and J_{NO} complexes, in which two B atoms in SW-BNNTs are replaced by two C atoms, are most stable ones. Thus, the best adsorption site for NO gas molecule in 2C-doped SW-BNNTs found to be above the slanted C-C bond located between pentagon and heptagon rings. After J_{ON} and J_{NO} complexes, I_{ON} and I_{NO} complexes (in which vertical C-C bond between two pentagon rings is involved in interaction) are energetically favorable. From calculated AEs, the stability order of $N_{ad}O_{ad}$ complexes is $J > I > H$.

To confirm the results obtained using ONIOM model, adsorption energies of 2C-doped SW-BNNT complexes were calculated after full optimization of complexes. The AEs resulted using this approach for **H** and **J** complexes are 5.1 and -11.5 kcal/mol, respectively that are nearly close to the AEs found using ONIOM model.

Adsorptions of NO molecule on (8,0) CNTs and BNNTs as well as SiCNT have been investigated by Gao *et al.*⁴⁵ They have shown that in contrast to CNTs and BNNTs, the SiCNTs exhibit highly exothermic binding to NO (-14.3 kcal/mol). The AE calculated⁴⁷ for the most stable NO-undoped SW-BNNT complex is ≈ -3.5 kcal/mol that smaller than those of found in this work for 2C-doped SW-BNNTs (-11.53 kcal/mol for **J_{ON}** and -10.35 for **J_{NO}** kcal/mol). Therefore, although adsorption of NO molecule on some sites of 2C-doped SW-BNNT is energetically unfavorable, our findings imply that the 2C-doped SW-BNNTs can be practically useful for the removal of NO molecule and as a sensor for detection of NO molecule.

When NO molecule is adsorbed on the NT, structural parameters of adsorbent and adsorbate species change. These structural deformations in NT are attributed to the change from sp^2 to sp^3 hybridization of the C atoms. The selected structural parameters are given in Fig. 5. The results obtained for 1C-doped SW-BNNTs show that the NO molecule prefers to lie on top of C atom. The N–O bond (1.147 Å in free molecule) is elongated upon adsorption so that its bond length in most stable **F_{NO}** and **G_{NO}** is 1.205 Å and 1.193 Å, respectively. The results show that the N–C bond in **F_{NO}** is shorter than O–C bond in **F_{ON}**, in good agreement with the greater AE obtained for **F_{NO}**. A similar situation is observed for **G** model. There is a direct correlation between NT–NO distance and AEs. Also it is interesting to notes that the NO–NT distance is significantly reduced when compared with the molecule on the un-doped SW-BNNT⁴⁷ in which NO molecule is perpendicular to tube surface.

For 2C-doped SW-BNNTs, results show that the NO molecule prefers to lie on top of C–C bonds and parallels to the surface of NT. Accordingly, NO molecule in most stable complexes adopts the parallel pattern on C–C sites. The N–O bond (1.147 Å in free molecule) is elongated upon adsorption so that its bond length in most stable J_{ON} and J_{NO} complexes (1.375 Å) is smaller than other ones. In addition, C–C bonds involved in interactions are weakened after adsorption of NO molecule. As can be seen, in contrast to NO–NT distance, elongation of C–C bond in most stable complexes is greater than other ones. The results show that the N–C bond in all 2C-doped complexes is longer than O–C bond. As observed for NO-SiCNT complexes,⁴⁵ there is no direct correlation between NT–NO distance and AEs. The results show that the bond lengths of N–C and O–C in most stable **J** complexes are greater than other ones. Also it is interesting to note that the NO–NT distance is significantly reduced when compared with the molecule on the undoped SW-BNNT⁴⁷ in which NO molecule is perpendicular to tube surface. Due to NO adsorption, the C atoms are slightly detached from the BNNT surface and, in turn, corresponding C–N or C–B bonds of NT are slightly elongated. The results of full optimization given in Fig. 6 are in good agreement with those of obtained using ONIOM approach.

Upon adsorption of NO on the nanotube surface, some charge is transferred from the HOMO of C-doped NT to the $2\pi^*$ orbital of NO, resulting in the changes in electronic properties of NT. To determine the amount of charge transferred between NO and NT, the charge transfer values were calculated through the NBO⁷⁹ charge difference between the adsorbed molecule on the NT surface and an isolated NO molecule. The CT values calculated at M06-2X/6-31++G(d,p) level of theory are given in Table 5. The negative value of CT (with exception of that found in I_{NO-O}) indicates that the charge is transferred from NT to NO molecule. The charge transferred from NT to NO molecule in most stable complexes J_{ON} and J_{NO} is 0.427 and 0.429 au, respectively. It is clear that CT values for the most stable

configurations are maximum, in good agreement with the greatest AEs found for these complexes. The less stable complexes have small CT and AE values.

The HOMO, LUMO and band gap energies (E_{gap}) of **H–N** complexes are also given in Table 6. Comparison of E_{gap} given in Table 5 (calculated at M06-2X/6-31+G(d) level) and those of listed in Table 6 (calculated at M06-2X/6-31++G(d,p) level), shows that the E_{gap} decreases as the basis set is improved. The results reveal that there is no definite trend in the change of the band gap as a function of AE of adsorbed molecule. It is clear that E_{gap} for most stable complexes is greater than others. The similar results have been observed for adsorption of NO molecule on the SiCNT⁴⁵. To confirm the E_{gap} values calculated using ONIOM method, E_{gap} in H_{NO} and J_{ON} were calculated using full optimized geometry obtained at M06-2X/6-31++G(d,p) level of theory. As can be seen in Table 6, E_{gap} values for H_{ON} and G_{NO} are 5.19 and 6.37 eV that are very close to those found using ONIOM geometry (5.36 and 6.56 eV).

In order to investigate the impact of number of doping sites on the adsorption properties of C-doped SW-BNNTs, 3C-doped nanotubes were also examined. For 3C-doped SW-BNNTs, twelve chemisorbed species were found in four groups **K**, **L**, **M** and **N**. The optimized structures are given in Fig. 5. The adsorption energies (AEs), HOMO, LUMO and band gap energies CT values are given in Table 5. The calculated AEs range from -5.0 to -29.6 kcal/mol for **K**, 24.6 to -29.4 kcal/mol for **L**, 11.78 to -29.4 kcal/mol for **M**, and -5.8 to -31.7 kcal/mol for **N** configurations. Comparison of AEs shows that the K_{ON} in **K** group, $\text{L}_{\text{NO-1}}$ in **L** group, $\text{M}_{\text{NO-1}}$ in **M** group and N_{ON} in **N** group are most stable complexes. Among the NO-3C-doped SW-BNNTs, N_{ON} chemisorbed complex with AE of -31.7 kcal/mol is most stable one. As mentioned previously, three B atoms in **N** nanotube are replaced by three C atoms. Comparison of AE in 2C-doped and 3C-doped NTs reveals that the best adsorption site for NO gas molecule in 3C-doped and 2C-doped SW-BNNTs is above the slanted C–C

bond located between pentagon and heptagon rings. In both most stable complexes \mathbf{N}_{ON} and \mathbf{J}_{ON} , only B atoms are replaced by C atoms, indicating that the doping structures are similar in both adsorbed complexes.

The ONIOM(M06-2X/6-31++(d,p):M06-2X/STO-6G) optimized structures of 3C-doped SW-BNNTs are also listed in Fig. 5. The N–O bond length in different complexes is greater than that of isolated one (1.147 Å). Increase in N–O bond length upon adsorption for most stable complex of each series is greater than others. In addition, the C–C bond length of doped NT involved in interaction shows a significant increase upon adsorption of NO molecule. In 3C-doped NTs, There is no a correlation between AEs and C–C as well as NO–NT distances. Also it is interesting to compare the distance between the NO and NT in most stable configurations of 2C- and 3C-doped NTs. As can be seen in Table 5, N–C and O–C distances in 3C-doped NT is smaller than that of 2C-doped one, although AEs of complexes have no significant difference.

The NBO results show that both N and O atoms have negative charges. The CT value calculates from sum of negative charges of N and O atoms are given in Table 5. As shown in this table, the charge transferred from NT to NO molecule in complexes having negative AE is considerable. In some less stable complexes, for example in $\mathbf{M}_{\text{NO-1}}$, owing to stretching the C–C bond (bond length is 2.573 Å) and position of N and O atoms on top of C–C bond, charge transferred from NT to N and O atoms is greater than those of found in most stable complexes. Thus, NBO population analysis confirms that greater elongation of C–C bond in $\mathbf{M}_{\text{NO-1}}$ complex.

The band gap energies for 3C-doped SW-BNNT–NO complexes are given in Table 5. Similar to 2C-doped NTs, there is no a definite trend in change of band gap. However, E_{gap} for most stable complex \mathbf{N}_{ON} is greatest.

4. Conclusions

By means of DFT methods, the effects of C-doping on the structural and electronic properties of SW-BNNTs as well as adsorption sensitivity of C-doped SW-BNNTs toward NO gas are explored. The results indicate that C substitution for B is favored over C substitution for N. The maximum value defect formation energy corresponds to the replacement of three carbon atoms with three nitrogen atoms that there are in pentagon rings of SW defect. It is predicted that increase in conductivity of C_B complexes is greater than C_N ones. The substituting C for B atom can modify the electronic structures of the SW-defective BNNTs by introducing C states into their band gaps and can thus make these nanotubes more reactive. The Fermi levels move to a high energy region when boron atoms are substituted with the carbon atoms in (6,0) SW-BNNT. The results show that the adsorption of NO on the some configurations of 2C- and 3C-doped SW-BNNTs is energetically favorable.

References

- 1 D. Golberg, Y. Bando, Y. Huang, T. Terao, M. Mitome, C. Tang, and C. Zhi, Boron Nitride Nanotubes and Nanosheets, *ACS Nano*, 2010, **4**, 2979–2993.
- 2 X. Blase, A. Rubio, S. G. Louie, and M. L. Cohen, , Stability and Band Gap Constancy of Boron Nitride Nanotubes, *Europhysics Letters*, 1994, **28**, 335.
- 3 N.G. Chopra, R. J. Luyken, K. Cherrey, V. H. Crespi, M. L. Cohen, S. G. Louie, and A. Zettl, Boron Nitride Nanotubes, *Science*, 1995, **269**, 966–967.
- 4 G. G. Fuentes, E. Borowiak-Palen, T. Pichler, X. Liu, A. Gra, G. Behr, J. Kalenczuk, M. Knupfer, and J. Fink, Electronic structure of multiwall boron nitride nanotubes, *Phys. Rev. B*, 2003, **67**, 035429.
- 5 G.Y. Guo, and J.C. Lin, Systematic ab initio study of the optical properties of BN nanotubes, *Phys. Rev. B*, 2005, **71**, 165402.
- 6 L. F. He, J. Shirahata, H. Suematsu, T. Nakayama, T. Suzuki, W. Jiang, and K. Niihara, Synthesis of BN nanosheet/nanotube-Fe nanocomposites by pulsed wire discharge and high-temperature annealing, *Materials Letters*, 2014, **117**, 120-123.
- 7 Y. Q. Zhang, Y. J. Liu, Y. Liu, and J. X. Zhao, Boosting sensitivity of boron nitride nanotube (BNNT) to nitrogen dioxide by Fe encapsulation, *Journal of Molecular Graphics and Modelling*, 2014, **51**, 1-6.
- 8 M. D. Esrafil, and N. Roghaye, A DFT study on the possibility of using boron nitride nanotubes as a dehydrogenation catalyst for methanol, *Applied Surface Science*, *Applied Surface Science*, 2014, **314**, 90-96.
- 9 R. Chegel, and B. Somayeh, Electro-optical properties of zigzag and armchair boron nitride nanotubes under a transverse electric field: Tight binding calculations, *Journal of Physics and Chemistry of Solids*, 2012, **73.2**, 154-161.
- 10 A. Freitas, S. Azevedo, and J. R. Kaschny, Effects of a transverse electric field on the electronic properties of single- and multi-wall BN nanotubes, *Solid State Communications*, 2013, **15**, 40–45.
- 11 H. Roohi, and S. Bagheri, Effect of axial strain on structural and electronic properties of zig-zag type of boron nitride nanotube (BNNT): a quantum chemical study, *Struct. Chem*, 2013, **24**, 409–420.

-
- 12 Z. G. Wang, Z. Li, and D. M. Cheng, Effects of uniaxial strain on the band structure of boron nitride nanotubes: A First Principle Study, *The European Physical Journal Applied Physics*, 2009, **46.02**, 20601.
- 13 Y. F. Zhukovskii, S. Piskunov, J. Begens, J. Kazeroovskis, and O. Lisovski, Geometries and stabilities of transition metals doped perfect and Stone–Wales defective armchair (5,5) boron nitride nanotubes, *physica status solidi (b)*, 2013, **250**, 793-800
- 14 S. Tontapha, N. Morakot, V. Ruangpornvisuti, and B. Wannoo, Boron Nitride Nanotubes Chemically Functionalized with Glycol Chitosan for Gene Transfection in Eukaryotic Cell Lines, *Structural Chemistry*, 2012, **23**, 1819-1830.
- 15 T. H. Ferreira, L. M. Hollanda, M. Lancellotti, and E. M. B. de Sousa, Boron Nitride Nanotubes, *J. Biomed Mater Res A*, 2015, **103**, 2176-2185.
- 16 C. Zhi, Y. Bando, C. Tang, and D. Golberg, *Mater. Sci. Eng. R*, 2010, **70**, 92–111.
- 17 L. Silva, S. Guerini, V. Lemos, J. Filho, Electronic and Structural Properties of Oxygen Doped BN Nanotubes, *IEEE Trans. Nanotechnol*, 2006, **5**, 517–522.
- 18 H. Liu and C. H. Turner, Adsorption properties of nitrogen dioxide on hybrid carbon and boron-nitride nanotubes, *Phys. Chem. Chem. Phys*, 2014, **16**, 22853-22860.
- 19 J. X. Zhao, and Y. H. Ding, Theoretical Study of Ni Adsorption on Single-Walled Boron Nitride Nanotubes with Intrinsic Defects, *J. Phys. Chem. C*, 2008, **112**, 5778–5783.
- 20 Y. Xie, and J. M. Zhang, First-principles study on substituted doping of BN nanotubes by transition metals V, Cr and Mn, *Comput. Theor. Chem*, 2011, **976**, 215–220.
- 21 Y. F. Zhukovskii, S. Piskunov, J. Kazeroovskis, D. Makaev, and P. Dyachkov, Comparative Theoretical Analysis of BN Nanotubes Doped by Al, P, Ga, As, In, and Sb, *J. Phys Chem C*, 2013, **117**, 14235–14240.
- 22 H. F. Bettinger, T. Dumitrica, G. E. Scuseria, and B. I. Yakobson, Mechanically induced defects and strength of BN nanotubes, *physical review B*, 2001, **65**, 041406.
- 23 C. Tang, Y. Bando, Y. Huang, S. L. Yue, C. Z. Gu, and F. F. Xu, Fluorination and Electrical Conductivity of BN Nanotubes, *J. Am. Chem. Soc*, 2005, **127**, 6552–6553.
- 24 O. Stephan, P. M. Ajayan, C. Colliex, P. Redlich, Doping Graphitic and Carbon Nanotube Structures with Boron and Nitrogen, *J. M. Lambert, P. Bernier, and P. Lefin, Science*, 1994, **266**, 1683–1685.

-
- 25 D. Golberg, Y. Bando, P. Dorozhkin, and Z. C. Dong, Synthesis, Analysis, and Electrical Property Measurements of Compound Nanotubes in the B-C-N Ceramic System, *MRS Bull*, 2004, **29**, 38–42.
- 26 L. Ci, L. Song, C. Jin, D. Jariwala, D. Wu, Y. Li, A. Srivastava, Z. F. Wang, K. Storr, L. and M. B. alicas, Atomic Layers of Hybridized Boron Nitride and Graphene Domains, *Nat. Mater*, 2010, **9**, 430–435.
- 27 O. L. Krivanek, O. L. Krivanek, M. F. Chisholm, V. Nicolosi, T. J. Pennycook, G. J. Corbin, N. Dellby, M. F. Murfitt, C. S. Own, Z. S. Szilagy, M. P. Oxley, S. T. Pantelides, and S. J. Pennycook, Atom-by-atom structural and chemical analysis by annular dark-field electron microscopy, *Nature*, 2010, **464**, 571.
- 28 X. Wei, M. Wang, Y. Bando, and D. Golberg, Post-Synthesis Carbon Doping of Individual Multiwalled Boron Nitride Nanotubes via Electron-Beam Irradiation, *J. Am. Chem. Soc*, 2010, **132**, 13592.
- 29 X. Wei, M. Wang, Y. Bando, and D. Golberg, Electron-Beam-Induced Substitutional Carbon Doping of Boron Nitride Nanosheets, Nanoribbons, and Nanotubes, *ACS Nano*, 2011, **5**, 2916.
- 30 A. J. Stone, and D. J. Wales, Theoretical Studies of Icosahedral C₆₀ and some Related Species, *Chemical Physics Letters*, 1986, **128**, 5.
- 31 T. Dumitrica, and B.I. Yakobson, Rate theory of yield in boron nitride nanotubes, *Phys. Rev. B*, 2005, **72**, 035418.
- 32 J. Choi, S. Pyo, D. H. Baek, J. I. Lee, and J. Kim, Thickness, alignment and defect tunable growth of carbon nanotube arrays using designed mechanical loads, *Carbon*, 2014, **66**, 126.
- 33 Y. Miyamoto, A. Rubio, S. Berber, M. Yoon, and D. Toanek, Spectroscopic characterization of Stone-Wales defects in nanotubes, *Phys. Rev. B*, 2004, **69**, 121413.
- 34 G. Kim, J. Park, and S. Hung, First principle study of substitutional carbon pair and Stone-Wales defect complexes in boron nitride nanotubes, *Chem. Phys. Lett*, 2012, **522**, 79-82 and references cited therein.
- 35 S. Jalili, F. Molani, M. Akhavan, and J. Schofield, Role of Defects on structural and electronic properties of zigzag C₃N nanotubes: A first-principle study, *Physica E*, 2014, **56**, 48–54.

- 36 M. Anafcheh, and R. Ghafouri, *J Clust, Carbon Doping of Defect Sites in Stone–Wales Defective Boron-nitride Nanotubes: A Density Functional Theory Study*, *Sci*, 2013, **24.3**, 865-879.
- 37 T. Roszer, *The biology of subcellular nitric oxide*, Springer Science & Business Media, 2012.
- 38 T. Fujitani, I. Nakamura, Y. Kobayashi, A. Takahashi, M. Haneda, and H. Hamada, Adsorption and reactions of NO on clean and CO-precovered Ir (111), *J. Phys. Chem. B*, 2005, **109**, 17603-17607.
- 39 C. Chang, G. Maduraiveeran, J. Xu, G. Hunter, and P. Dutta, Design, fabrication, and testing of MEMS-based miniaturized potentiometric nitric oxide sensors, *Sens. Actuators, B*, 2014, **204**, 183-189.
- 40 C. S. Yeung, Y. K. Chen, Y. A. Wang, *Sensors, Defected and Substitutionally Doped Nanotubes: Applications in Biosystems, Sensors, Nanoelectronics, and Catalysis*, 2011.
- 41 O. Byl, P. Kondratyuk, and J. Yates, Adsorption and Dimerization of NO Inside Single-Walled Carbon Nanotubes An Infrared Spectroscopic Study, *J. Phys. Chem. B*, 2003, **107**, 4277-4279.
- 42 T. Kyotani, and A. Tomita, Analysis of the reaction of carbon with NO/N₂O using ab initio molecular orbital theory, Electronic properties of adsorption nitrogen monoxide on inside and outside of the armchair single wall carbon nanotubes: a density functional theory calculations, *J. Phys. Chem. B*, 1999, **103**, 3434-3441.
- 43 A. A. Rafati, S. M. Hashemianzadeh, and Z. B. Nojini, Adsorption of CO and NO molecules on carbon doped boron nitride nanotubes, *J. Phys. Chem. C*, 2008, **112**, 3597-3604.
- 44 R. J. Baierle, T. M. Schmidt, and A. Fazzio, Adsorption of CO and NO molecules on carbon doped boron nitride nanotubes, *Solid State Communications*, **2007**, 142, 49–53.
- 45 G. Gao, and H. S. Kang, First principles study of NO and NNO chemisorption on silicon carbide nanotubes and other nanotubes, *J. Chem. Theory Comput*, 2008, **4**, 1690-1697.
- 46 Y. Chen, Y. J. Liu, H. X. Wang, J. X. Zhao, Q. Cai, X. Z. Wang, and Y. Ding, Silicon-doped graphene: an effective and metal-free catalyst for NO reduction into N₂O?, *ACS Appl. Mater. Interfaces*, 2013, **5**, 5994-6000.
- 47 H. Roohi, and M. Jahantab, Adsorption sensitivity of the perfect and Stone–Wales defective BNNTs towards NO gas: A DFT study, *J. Mol. Graph. Model.* submitted.

- 48 H. Roohi, A. R. Nowroozi, A. Ebrahimi, and B. Makiabadi, Effect of CH₃CO functional group on the molecular and electronic properties of BN_{43zz} nanotube: A computational chemistry study, *Journal of Molecular Structure (THEOCHEM)*, 2010, **952**, 36–45.
- 49 H. Roohi, M. Jahantab, and M. Yakta, Effect of the Stone–Wales (SW) defect on the response of BNNT to axial tension and compression: a quantum chemical study, *Struct. Chem*, 2015, **26(1)**, 11–22
- 50 H. Roohi, and S. Khyrkhah, Green chemical functionalization of single-wall carbon nanotube with methylimidazolium dicyanamid ionic liquid: A first principle computational exploration, *Journal of Molecular Liquids*, 2015, **211**, 498–505.
- 51 H. Roohi, M. Jahantab, S. Rahmdel Delcheh, and B. Pakdel Khoshakhlagh, Chemical functionalization of boron nitride nanotube via the 1,3-dipolar cycloaddition reaction of azomethine ylide: A quantum chemical study, *Strut. Chem*. 2015, **26(3)**, 749–759.
- 52 A. D. Becke, A new mixing of Hartree-Fock and local density-functional theories, *J. Chem. Phys*, 1993, **98**, 5648–5672.
- 53 C. Lee, W. Yang, and R. G. Parr, Development of the Colic-Salvetti correlation-energy formula into a functional of the electron density, *Phys. ReV. B*, 1988, **37**, 785–789.
- 54 M. J. Frisch, G. W. Trucks, H. B. Schlegel, G. E. Scuseria, M. A. Rob, J. R. Cheeseman, J. A. Montgomery Jr., T. Vreven, K. N. Kudin, J. C. Burant, J. M. Millam, S. S. Iyengar, J. Tomasi, V. Barone, B. Mennucci, M. Cossi, G. Scalmani, N. Rega, G. A. Petersson, H. Nakatsuji, M. Hada, M. Ehara, K. Toyota, R. Fukuda, J. Hasegawa, M. Ishida, T. Nakajima, Y. Honda, O. Kitao, H. Nakai, M. Klene, X. Li, J. E. Knox, H. P. Hratchian, J. B. Cross, V. Bakken, C. Adamo, J. Jaramillo, R. Gomperts, R. E. Stratmann, O. Yazyev, A. J. Austin, R. Cammi, C. Pomelli, J. W. Ochterski, P. Y. Ayala, K. Morokuma, G. A. Voth, P. Salvador, J. J. Dannenberg, V. G. Zakrzewski, S. Dapprich, A. D. Daniels, M. C. Strain, O. Farkas, D. K. Malick, A. D. Rabuck, K. Raghavachari, J. B. Foresman, J. V. Ortiz, Q. Cui, A. G. Baboul, S. Clifford, J. Cioslowski, B. B. Stefanov, G. Liu, A. Liashenko, P. Piskorz, I. Komaromi, R. L. Martin, D. J. Fox, T. Keith, M. A. Al-Laham, C. Y. Peng, A. Nanayakkara, M. Challacombe, P. M. W. Gill, B. Johnson, W. Chen, M. W. Wong, C. Gonzalez, and J. A. Pople, *Gaussian 03*, (Gaussian, Inc., Wallingford, CT, 2003).
- 55 M. W. Schmidt, K. K. Baldridge, J. A. Boatz, S. T. Elbert, M. S. Gordon, J. H. Jensen, S. Koseki, N. Matsunaga, K. A. Nguyen, S. Su, T. L. Windus, M. Dupuis, and J. A. Montgomery, General Atomic and Molecular Electronic Structure System, *J. Comput. Chem*, 1993, **14**, 1347–1363.

-
- 56 T. Lu, and F. Chen, *J. Comput. Chem.*, 2012, **33**, 580.
- 57 D. A. Neamen, and Fourth Edition, *Semiconductor Physics and Devices Basic Principles*, Fourth Edition, McGraw-Hill, 2011, 784 .
- 58 R. G. Parr, and W. Yang, *Density functional theory of atoms and molecules*, Oxford University Press, New York, 1989.
- 59 P. Geerlings, F. De Proft, and W. Langenaeker, *Conceptual density functional theory*, *Chem Rev*, 2003, **103**, 1793–1874.
- 60 R. K. Roy, and S. Saha, *Studies of regioselectivity of large molecular systems using DFT based reactivity descriptors*, *Ann Rep C*, 2010, **106**, 106-118.
- 61 E. P. Gyftopoulos, and G. N. Hatsopoulos, *Quantum-thermodynamic definition of electronegativity*, *Proc Natl Acad Sci USA*, 1968, **60**, 786.
- 62 R. G. Parr, R. A. Donnelly, M. Levy, and W. E. Palke, *Electronegativity-the density functional viewpoint*, *J Chem Phys*, 1978, **68**, 380.
- 63 R. G. Parr, and R. G. Pearson, *Absolute hardness: companion parameter to absolute electronegativity*, *J Am Chem Soc*, 1983, **105**, 7512–7516.
- 64 T. Koopmans, *U ber die Zuordnung von Wellenfunktionen und Eigenwerten zu den Einzelnen Elektronen Eines Atoms*, *Physica*, 1934, **1**, 104–113.
- 65 R. G. Parr, L. Szentpaly, and S. Liu, *Electrophilicity index*, *J Am Chem Soc*, 1999, **121**, 1922–1924.
- 66 T. Vreven, K. S. Byun, I. Komáromi, S. Dapprich, J. A. Montgomery Jr., K. Morokuma, and M. J. Frisch, *Combining quantum mechanics methods with molecular mechanics methods in ONIOM,” J. Chem. Theory and Comput.*, 2006, **2**, 815-26.
- 67 T. Vreven, L. M. Thompson, S. M. Larkin, I. Kirker, M. J. Bearpark, *Deconstructing the ONIOM Hessian: Investigating Method Combinations for Transition Structures*, *J. Chem. Theory Comput.* 2012, **8**, 4907–4914.
- 68 L. V. Liu, W. Q. Tian, Y. A. Wang, *Ozonization at the Vacancy Defect Site of the Single-Walled Carbon Nanotube*, *J. Phys. Chem. B*, 2006,**110**,13037-1304.
- 69 H. Choi, Y. C. Park, Y.-H. Kim, Y. S. Lee, *Ambient Carbon Dioxide Capture by Boron-Rich Boron Nitride Nanotube*, *J. Am. Chem. Soc.* 2011, **133**, 2084–2087
- 70 Y. Li, Z. Zhou, D. Colberg, Y. Bando, P. v. R. Schleyer, and Z. Chen, *Ston-Wa;es defects in single-walled boron nitride nanotubes: Formation energies, electronic structures and reactivity*, *J Chem Phys C*, 2008, **112**, 1365.

-
- 71 P. Piquini, R. J. Baierle, T. M. Schmidt, and A. Fazio, Formation energy of native defects in BN nanotubes: an ab initio study, *Nanotechnol*, 2005, **16**, 827.
- 72 T. Zhao, J. Shi, M. Huo, and R. Wan, Electronic properties of C-doped boron nitride nanotubes studied by first-principles calculations, *Physica E*, 2014, **64**, 123–128.
- 73 Y. K. Chen, L. V. Liu, and Y. A. Wang, Density Functional Study of Interaction of Atomic Pt with Pristine and Stone-Wales-Defective Single-Walled Boron Nitride Nanotubes, *J. Phys. Chem. C*, 2010, **114**, 12382–12388.
- 74 C. Kittel, and H. Kroemer, *Thermal Physics*, W. H. Freeman, 1980, 363.
- 75 R. A. Swalin, *Thermodynamics of Solids*, Wiley. Day, 1972, **8**, 244.
- 76 Y. Xi, X. Zhao, A. Wang, X. Wang, H. Bu, and M. Zhao, Tuning the electronic and magnetic properties of triangular boron nitride quantum dots via carbon doping, *Physica E*, 2013, **49**, 52–60.
- 77 J. X. Zhao, and B. Q. Dai, DFT studies of electro-conductivity of carbon-doped boron nitride nanotube, *Materials Chemistry and Physics*, 2004, **88**, 244–249.
- 78 R.G. Pearson, *Hard and soft acids and bases*, Dowden. Hutchison & Ross, Stroudsburg, PA, 2001.
- 79 E. D. Glendening, A. E. Reed, J. E. Carpenter, F. A. Weinhold, Department of Chemistry, University of California-Irvine, Irvine, CA. NBO, 1995, 3.1.

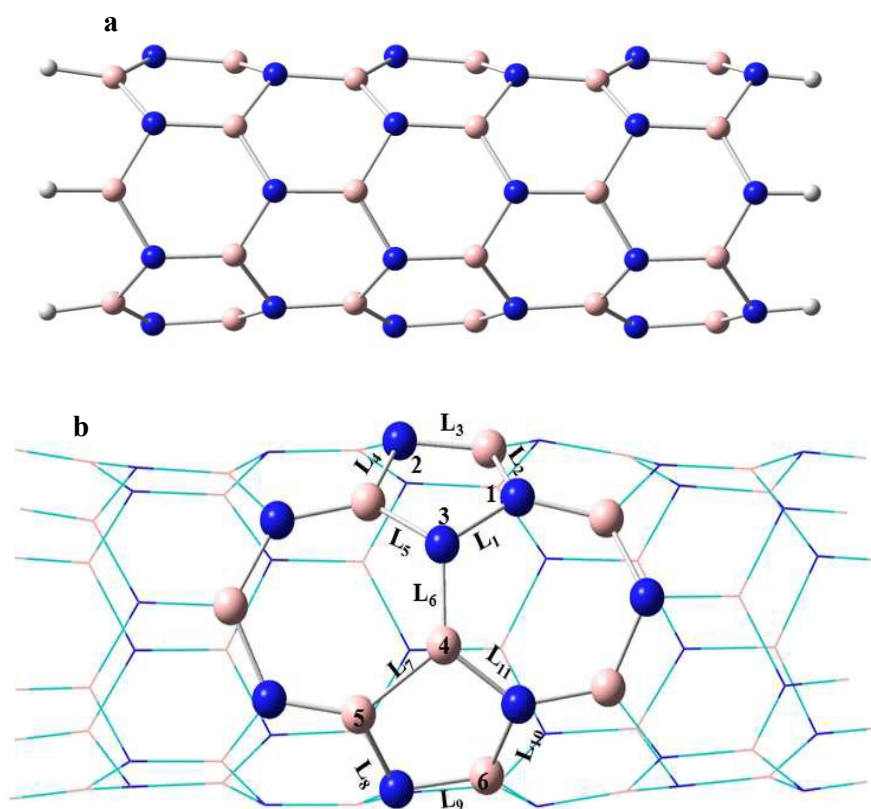


Fig. 1. (a) Pristine (6,0) BNNT (**D**) and (b) Schematic representation to SW defective (6,0) BNNT (**E**). 1C doped SW-BNNTs that one carbon atom substituted in 3 and 4 positions named as **F_N** and **G_B**, two carbon atoms substituted in three different situations (1,3), (3,4) and (4,5) denoted as **H₁₃**, **I₃₄** and **J₄₅** and three carbon atoms substituted in four different situations (1,2,3), (1,3,4), (3,4,5) and (4,5,6) symbolized as **K₁₂₃**, **L₁₃₄**, **M₃₄₅** and **N₄₅₆**, respectively. Blue and pink spheres represent N and B atoms, respectively.

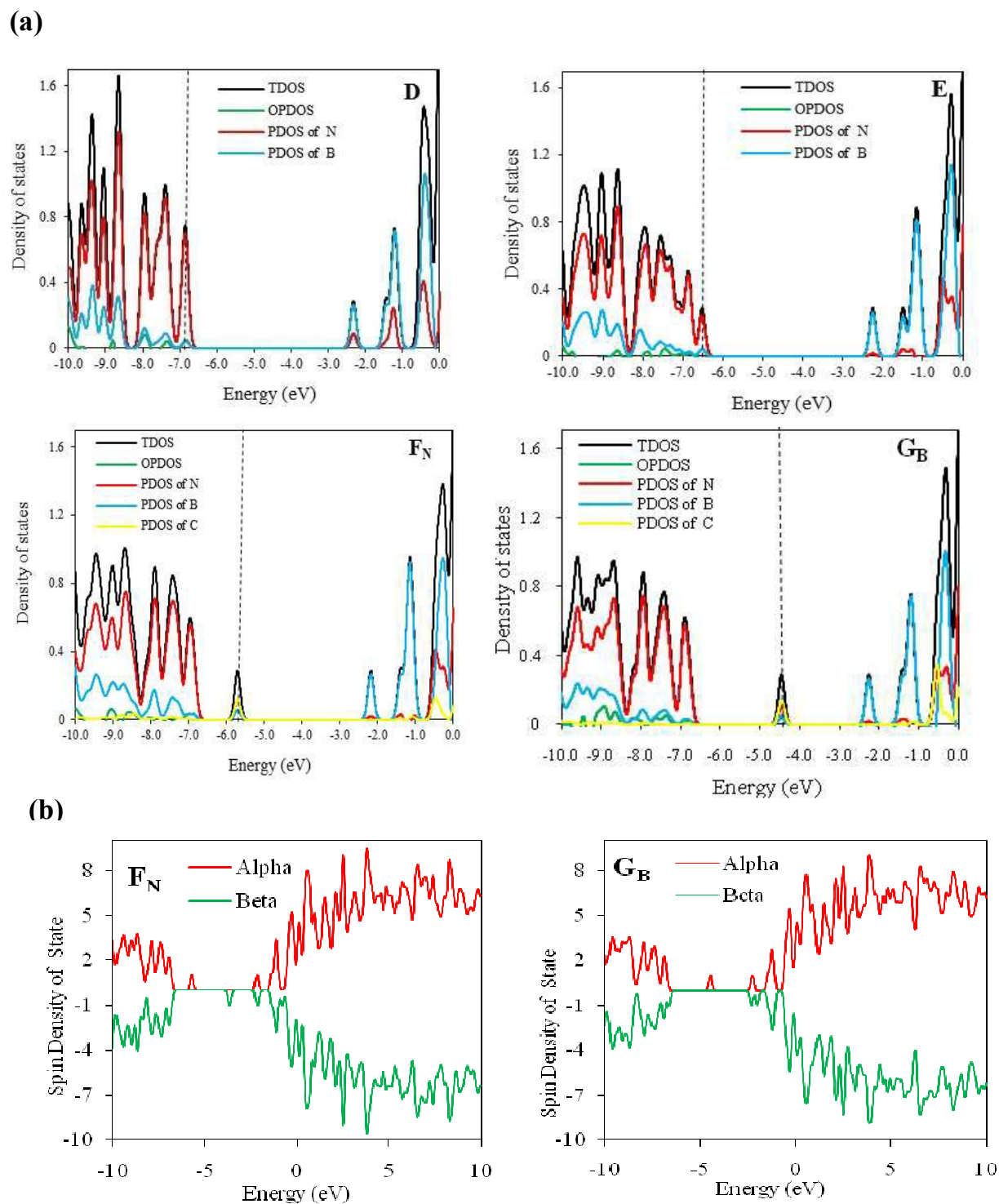


Fig. 2. (a) Density of states (DOS) of **D**, **E**, **F_N**, and **G_B** models. Black and green curves indicate the total DOS and, whereas red, blue, and yellow curves indicate DOS of N, B, and C and partial DOS, respectively. Black vertical dashed lines mark the Fermi levels. (b) Calculated total spin DOSs for the **F_N** and **G_B** 1C-doped SW-BNNTs.

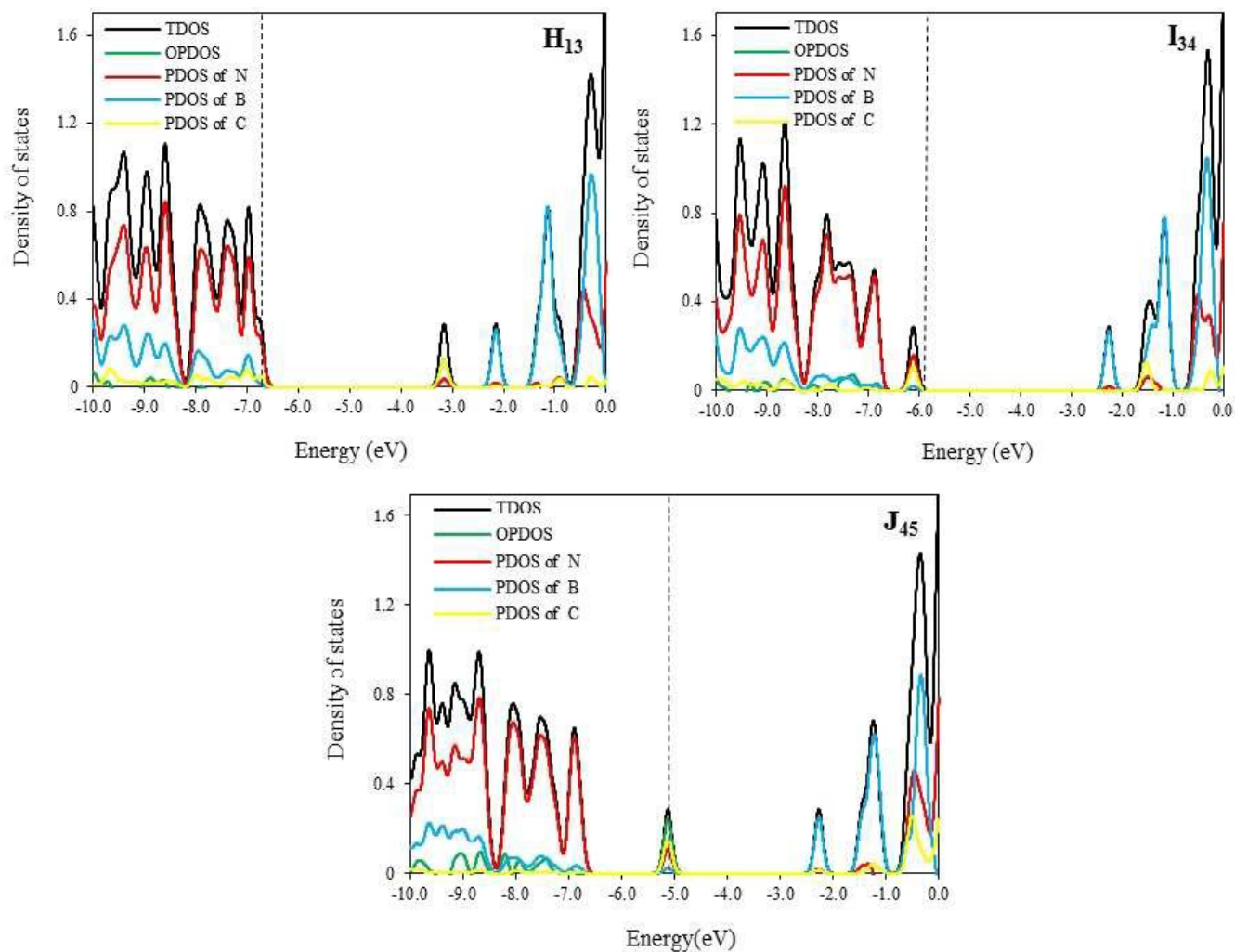


Fig. 3. Plotted density of states (DOS) of H_{13} , I_{34} , and J_{45} models. Black and green curves indicate, respectively, the total DOS and overlap population density of states (OPDOS), whereas red, blue and yellow curves indicate partial DOS of N, B and C, respectively. Black vertical dashed lines mark the Fermi levels.

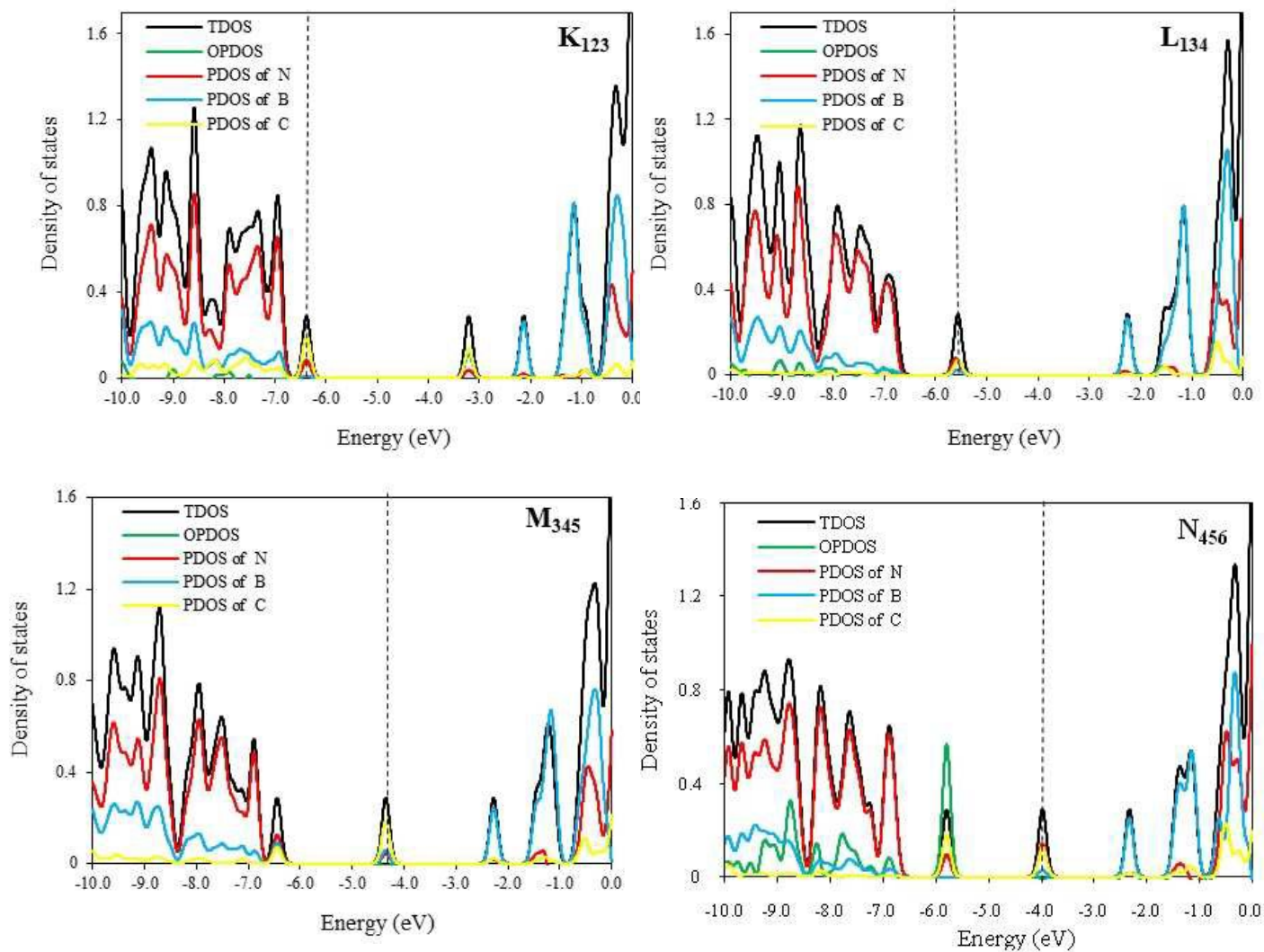


Fig. 4 Plotted total and projected density of states (DOS) of K_{123} , L_{134} , M_{345} , and N_{456} models. Black and green curves indicate, respectively, the total DOS and overlap population density of states (OPDOS), whereas red, blue and yellow curves indicate partial DOS of N, B and C, respectively. Black vertical dashed lines mark the Fermi levels.

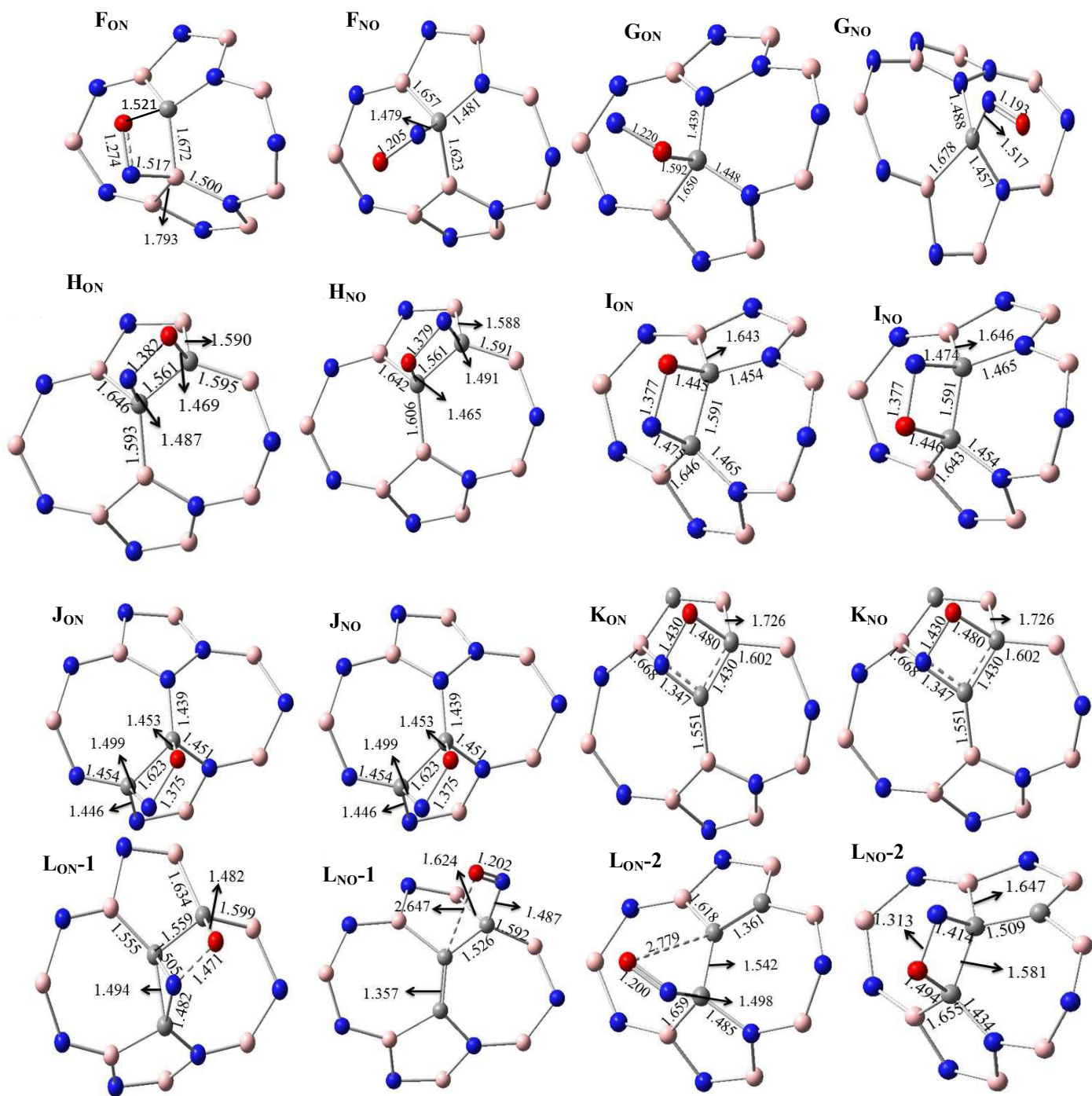


Fig. 5. Selected structural parameters of C-doped SW-BNNT complexes calculated at ONIOM(M06-2X/6-31++(d,p):M06-2X/STO-6G) level. Distances are given in Å.

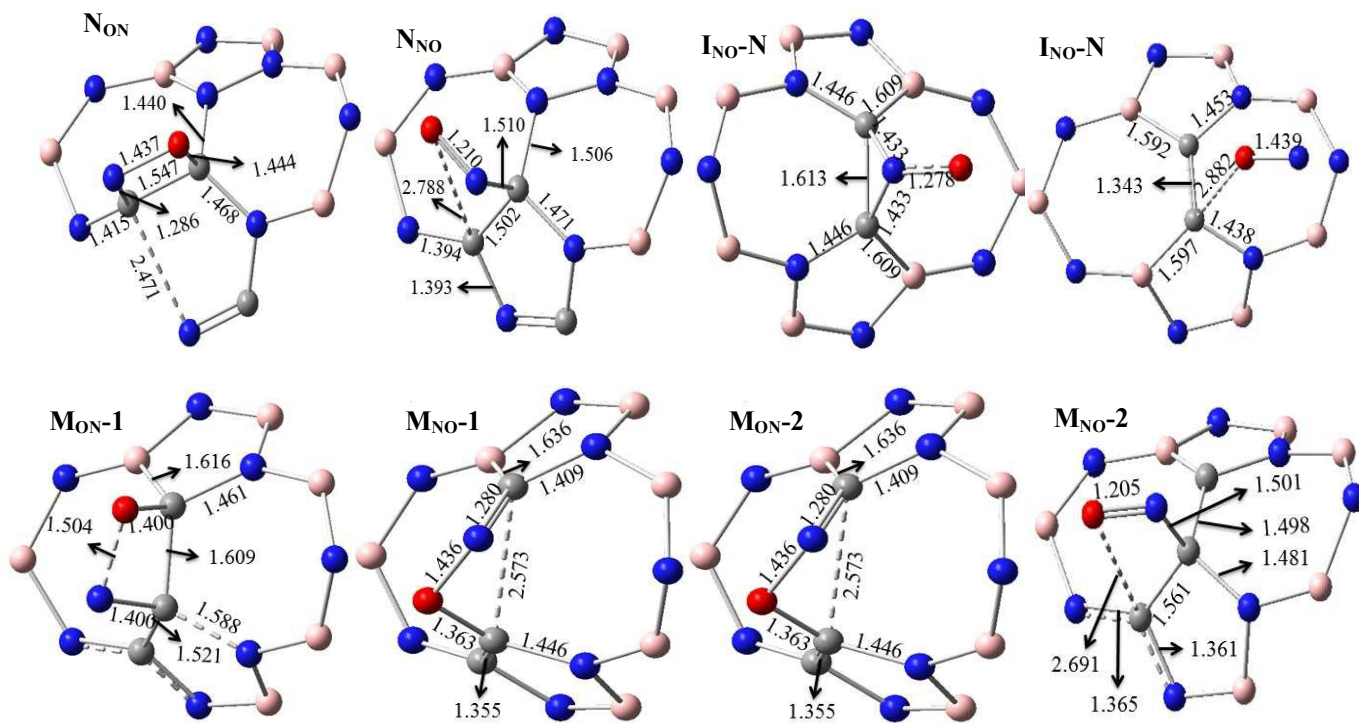


Fig. 5. Continued.

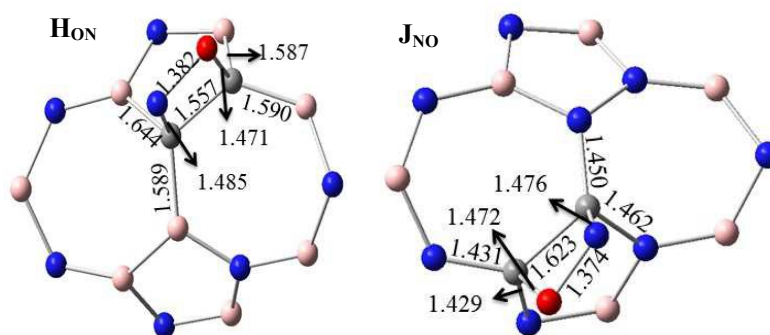


Fig. 6. Selected structural parameters of 2C-doped SW-BNNT complexes obtained using full optimization at the M06-2X/6-31++G(d,p) level. Distances are given in Å.

Table 1. The bond lengths (\AA) calculated at B3LYP/6-31+G(d) level for C₁₋₃-doped SW-BNNTs

BNNTs	L ₁	L ₂	L ₃	L ₄	L ₅	L ₆	L ₇	L ₈	L ₉	L ₁₀	L ₁₁
E	1.469	1.449	1.421	1.451	1.495	1.438	1.711	1.458	1.442	1.464	1.468
F_N	1.419	1.474	1.426	1.463	1.595	1.540	1.714	1.464	1.441	1.468	1.469
G_B	1.467	1.446	1.419	1.444	1.512	1.427	1.553	1.468	1.422	1.466	1.431
H₁₃	1.380	1.565	1.436	1.469	1.625	1.568	1.721	1.458	1.444	1.473	1.470
I₃₄	1.587	1.457	1.430	1.461	1.446	1.370	1.446	1.461	1.430	1.457	1.587
J₄₅	1.488	1.444	1.418	1.441	1.516	1.449	1.382	1.443	1.413	1.451	1.428
K₁₂₃	1.393	1.569	1.519	1.555	1.629	1.575	1.722	1.459	1.443	1.474	1.467
L₁₃₄	1.430	1.548	1.439	1.463	1.611	1.405	1.591	1.453	1.431	1.470	1.441
M₃₄₅	1.460	1.463	1.430	1.457	1.561	1.409	1.439	1.428	1.423	1.447	1.437
N₄₅₆	1.482	1.443	1.419	1.441	1.512	1.442	1.375	1.440	1.396	1.441	1.419

Table 2. Sum of the angles around 1 to 6 sites of C-doped SW-BNNTs computed at B3LYP/6-31+G(d) level

BNNTs	1	2	3	4	5	6
E	355.2	339.7	342.6	351.8	356.3	357.1
F_N	355.1	338.5	345.8	347.0	356.6	356.9
G_B	357.3	339.3	336.0	353.3	358.8	356.5
H₁₃	353.6	336.0	347.2	347.6	356.5	357.0
I₃₄	354.5	337.9	350.2	350.3	358.1	356.5
J₄₅	357.3	338.5	321.8	359.3	360.0	354.5
K₁₂₃	353.6	330.7	350.0	349.2	356.7	356.9
L₁₃₄	352.4	337.0	350.7	350.7	358.3	356.4
M₃₄₅	354.8	336.0	342.2	356.0	359.1	355.1
N₄₅₆	357.4	338.0	323.1	359.6	360.0	339.5

Table 3. Defect formation energy (E_{form}), HOMO (E_{H}), LUMO (E_{L}) and band gap (E_{g}) energies for D–N structures calculated using B3LYP and M06-2X methods

BNNTs	B3LYP				M06-2X			
	$E_{\text{form}}/\text{eV}$	$E_{\text{HOMO}}/\text{eV}$	$E_{\text{LUMO}}/\text{eV}$	E_{g}/eV	$E_{\text{form}}/\text{eV}$	$E_{\text{HOMO}}/\text{eV}$	$E_{\text{LUMO}}/\text{eV}$	E_{g}/eV
D	0.00	-6.83	-2.32	4.50	0.00	-8.30	-1.41	6.89
E	3.95	-6.52	-2.25	4.27	4.21	-7.94	-1.34	6.60
F_N	4.06	-5.71	-2.18	3.53	4.33	-6.92	-0.91	6.02
G_B	3.41	-4.46	-2.26	2.20	3.86	-5.67	-1.44	4.23
H₁₃	4.33	-6.75	-3.16	3.58	4.56	-8.18	-2.28	5.90
I₃₄	0.71	-6.12	-2.26	3.86	1.01	-7.38	-1.36	6.02
J₄₅	2.27	-5.12	-2.27	2.86	2.75	-6.36	-1.37	4.99
K₁₂₃	6.92	-6.39	-3.21	3.18	7.28	-7.74	-2.29	5.45
L₁₃₄	1.87	-5.56	-2.26	3.31	2.29	-6.71	-1.36	5.34
M₃₄₅	0.75	-4.35	-2.27	2.08	1.32	-5.37	-1.40	3.97
N₄₅₆	2.83	-3.98	-2.33	1.65	3.58	-5.17	-1.43	3.74

Table 4. The values of electronic chemical potential (μ), hardness (η), softness (S), electrophilicity index (ω), and dipole moment (Q) for **D** to **N** models

SW-BNNTs	μ /eV	η /eV	S/eV ⁻¹	ω /eV	Q/Debye
D	-4.58	2.25	0.44	4.65	6.54
E	-4.39	2.13	0.47	4.51	6.21
F_N	-3.94	1.76	0.57	4.41	7.20
G_B	-3.36	1.10	0.91	5.13	6.43
H₁₃	-4.95	1.79	0.56	6.85	7.17
I₃₄	-4.19	1.93	0.52	4.55	6.13
J₄₅	-3.70	1.43	0.70	4.78	6.23
K₁₂₃	-4.80	1.59	0.63	7.23	7.44
L₁₃₄	-3.91	1.65	0.60	4.62	6.23
M₃₄₅	-3.31	1.04	0.96	5.28	6.00
N₄₅₆	-3.15	0.82	1.22	6.05	5.52

Table 5. HOMO (E_H), LUMO (E_L), and band gap energies (E_g) of (F_N - N) models in eV calculated at M062X/6-31++G(d,p) level

	E_{HOMO}/eV	E_{LUMO}/eV	E_g/eV
F_N	-6.99	-1.15	5.84
G_B	-5.69	-1.27	4.42
H₁₃	-8.16	-2.33	5.83
I₃₄	-7.46	-1.23	6.23
J₄₅	-6.41	-1.25	5.16
K₁₂₃	-7.78	-1.10	6.67
L₁₃₄	-6.79	-1.23	5.56
M₃₄₅	-5.41	-1.28	4.13
N₄₅₆	-5.33	-1.31	4.02

Table 6. Adsorption energies (E_{ads}), HOMO (E_{HOMO}), LUMO (E_{LUMO}), band gap energies (E_{g}) the charges on the N and O atoms (q_{N} , q_{O}), and the total NBO charge on the NO molecule (CT_{NBO}) of various configurations of C-doped SW-BNNT-NO complexes in eV calculated after single point calculations using ONIOM approach. The data in parenthesis corresponds to full optimized models

	$E_{\text{ads}}/\text{kcal mol}^{-1}$	$E_{\text{HOMO}}/\text{eV}$	$E_{\text{LUMO}}/\text{eV}$	E_{g}/eV	$q_{\text{N}}/\text{a.u.}$	$q_{\text{O}}/\text{a.u.}$	CT_{NBO}
F_{ON}	-9.63	-8.03	-2.55	5.48	0.067	-0.214	-0.147
F_{NO}	-31.29	-7.91	-1.65	6.26	0.166	-0.312	-0.146
G_{ON}	6.96	-6.75	-1.31	5.44	-0.261	-0.039	-0.300
G_{NO}	-33.62	-7.70	-1.32	6.37	0.139	-0.261	-0.123
H_{ON}	4.55 (5.11)	-6.99 (-6.90)	-1.64 (-1.71)	5.36 (5.18)	-0.039	-0.357	-0.396
H_{NO}	5.11	-7.04	-1.8	5.23	-0.039	-0.354	-0.393
I_{ON}	-0.46	-7.78	-1.36	6.42	-0.043	-0.370	-0.413
I_{NO}	-0.47	-7.79	-1.37	6.42	-0.044	-0.370	-0.414
I_{NO(O)}	62.10	-7.46	-3.43	4.05	0.283	-0.276	0.007
I_{NO(N)}	2.05	-7.75	-1.31	6.44	-0.021	-0.325	-0.346
J_{ON}	-10.35	-8.01	-1.29	6.72	-0.045	-0.382	-0.427
J_{NO}	-11.53 (-11.5)	-7.88 (-7.83)	-1.32 (-1.46)	6.56 (6.37)	-0.043	-0.386	-0.429
K_{ON}	-29.59	-7.13	-2.48	4.65	-0.226	-0.332	-0.558
K_{NO}	-5.01	-7.26	-2.5	4.76	-0.244	-0.158	-0.086
L_{NO-1}	-29.36	-7.75	-1.34	6.41	-0.302	0.153	-0.149
L_{NO-2}	17.98	-6.94	-2.66	4.28	0.172	-0.284	-0.112
L_{ON-1}	24.63	-7.81	-1.33	6.49	-0.128	-0.373	-0.501
L_{ON-2}	-24.29	-7.99	-1.9	6.09	0.170	-0.291	-0.121
M_{NO-1}	-29.39	-6.69	-1.37	5.32	-0.149	-0.410	-0.559
M_{NO-2}	1.16	-5.9	-1.68	4.23	0.134	-0.320	-0.186
M_{ON-1}	11.78	-5.59	-2.01	3.57	-0.477	-0.422	-0.899
M_{ON-2}	-25.15	-7.59	-1.42	6.17	0.145	-0.258	-0.113
N_{ON}	-31.72	-7.98	-1.29	6.69	-0.093	-0.438	-0.531
N_{NO}	-5.61	-5.34	-1.35	3.99	0.088	-0.331	-0.243